Journal of Elasticity **60:** 173–221, 2000.

Theory of Supercoiled Elastic Rings with Self-Contact and Its Application to DNA Plasmids

BERNARD D. COLEMAN and DAVID SWIGON
Department of Mechanics and Materials Science, Rutgers, The State University of New Jersey, 98 Brett Road, Piscataway, NJ 08854-8058, U.S.A.

Dedicated to the memory of our teacher Clifford Truesdell. Would that we could meet the standard he set for clarity of expression!

Received 19 June 2000; in revised form 27 December 2000

Abstract. Methods are presented for obtaining exact analytical representations of supercoiled equilibrium configurations of impenetrable elastic rods of circular cross-section that have been pretwisted and closed to form rings, and a discussion is given of applications in the theory of the elastic rod model for DNA. When, as here, self-contact is taken into account, and the rod is assumed to be inextensible, intrinsically straight, transversely isotropic, and homogeneous, the important parameters in the theory are the excess link $\Delta\mathcal{L}$ (a measure of the amount the rod was twisted before its ends were joined), the ratio ω of the coefficients of torsional and flexural rigidity, and the ratio d of cross-sectional diameter to the length of the axial curve $\mathcal{C}$. Solutions of the equations of equilibrium are given for cases in which self-contact occurs at isolated points and along intervals. Bifurcation diagrams are presented as graphs of $\Delta\mathcal{L}$ versus the writhe of $\mathcal{C}$ and are employed for analysis of the stability of equilibrium configurations. It is shown that, in addition to primary, secondary, and tertiary branches that arise by successive bifurcations from the trivial branch made up of configurations for which the axial curve is a circle, there are families of equilibrium configurations that are isolas in the sense that they are not connected to bifurcation branches by paths of equilibrium configurations compatible with the assumed impenetrability of the rod. Each of the isolas found to date is connected to a bifurcation branch by a path which, although made up of solutions of the governing equations, contains regions on which the condition of impenetrability does not hold.

Mathematics Subject Classifications (2000): 74B20, 74K10, 74G60, 74M15, 92C40, 74G05.

Key words: contact problems for elastic rods, DNA topology.

1. Statement of the Problem

A long standing problem in Kirchhoff's nonlinear theory of elastic rods has been that of finding exact solutions of the equations of equilibrium for cases in which configurations can show isolated points and intervals of self-contact. We here treat the problem for the case of an impenetrable rod of circular cross-section that is inextensible, homogeneous, intrinsically straight, and transversely isotropic in elastic

response.* Throughout the paper the emphasis is on rods that have been pretwisted and circularly closed to form rings. In molecular biology such elastic rings serve as models for cyclized DNA segments, called *plasmids*.

A DNA molecule contains two complementary polynucleotide strands joined together in a duplex structure, i.e., a Watson–Crick double helix. Each strand has a sugar-phosphate backbone chain to which there are attached nucleotide bases of four types: A, T, C, G, with A complementary to T, and C complementary to G. In this duplex structure each base on one strand is bound to its complement on the other strand. The resulting base pairs are, in an approximate sense, flat, rigid, rectangular objects (like dominos). In B-DNA, the most common form of DNA, the base pairs are stacked so that they are roughly parallel with mid-planes separated by 3.4 Å, with their centers lying on a curve called the *duplex axis*, and with each base pair rotated relative to its predecessor by about one tenth of a full turn. We here assume that when a segment of DNA is stress-free its duplex axis is straight. In a plasmid each strand and the duplex axis are closed curves.

In a rough sketch, a segment of B-DNA would appear as a tube with an approximate diameter of 20 Å and with two parallel helical indentations, called the *major* and *minor grooves*, which have a pitch of circa 34 Å (or 10 base pairs) and a common axis that coincides with the duplex axis. The base pairs are in the interior of the tube, while the sugar-phosphate chains lie on its surface and constitute the material between the two helical grooves. The base pairs, or, equivalently, the bases on one of the two complementary strands, are the units of the genetic code. The original Watson–Crick value for the average pitch h of the helical structure is 10 base pairs; that value is appropriate to crystalline DNA; under physiological conditions h is closer to 10.5 base pairs.

We here employ a familiar idealized elastic rod model of the mechanics of duplex DNA which does not account for such details of DNA structure as the presence of grooves. Thus we treat a DNA segment as an impenetrable elastic tube of circular cross-section obeying the special case of Kirchhoff's theory of elastic rods [4–6] in which a rod is taken to be not only transversely isotropic but also inextensible.

Two kinematical concepts are of central importance in characterizing the state of a rod $\mathcal{R}$ of the type we consider: (i) the *axial curve* $\mathcal{C}$, which is the present locus in space of the material points that form the axis of $\mathcal{R}$ and which is described by

* Two recent papers [1, 2] on the elastic stability of DNA configurations contain preliminary announcements of some of the results presented here. In [1] the emphasis is on the derivation of criteria for stability and on configurations of DNA segments subjected to strong anchoring end conditions; in [2], as here, it is on configurations of plasmids. When only isolated points of self-contact are present, our method of solving the governing equations is that presented in the doctoral dissertation of Swigon [3]. A detailed description of the method and an extension of it to cases in which there are intervals as well as isolated points of self-contact are given in the present paper.

giving a function $\boldsymbol{x}(\cdot)$ of the arc-length parameter s; and (ii) the *twist density* Ω which is defined by the relation

$$\Omega = \Omega(s) = \boldsymbol{d}(s) \times \boldsymbol{d}'(s) \cdot \boldsymbol{t}(s), \quad 0 \leqslant s \leqslant L. \tag{1.1}$$

Here L is the (invariant) length of $\mathcal{R}$, $\boldsymbol{t}(s) = \boldsymbol{x}'(s) = \mathrm{d}\boldsymbol{x}(s)/\mathrm{d}s$ is the (unit) tangent vector of $\mathcal{C}$ at s, and $\boldsymbol{d}(s)$ is a unit vector imbedded in the cross-section at s.

Kirchhoff showed that there is a precise sense in which his general theory of rods is an approximation to a theory of a class of three-dimensional bodies.* In a deformation of the three-dimensional body approximated by $\mathcal{R}$, $\boldsymbol{d}(s)$ transforms as though it originates at the point $\boldsymbol{x}(s)$ and is tangent to a material fiber that lies in the cross-section at s. The value of $\boldsymbol{d}(s)$ in each configuration of $\mathcal{R}$ depends on the choice made for $\boldsymbol{d}_{\mathrm{u}}(s)$, the value of $\boldsymbol{d}(s)$ in an undistorted, stress-free, reference configuration.

A rod $\mathcal{R}$ is said to be *closed* (or "circularly closed") if, in each of its configurations, $\mathcal{C}$ is a closed curve and both $\boldsymbol{t}(\cdot)$ and $\boldsymbol{d}(\cdot)$ are continuous functions on $\mathcal{C}$. The closed rods $\mathcal{R}$ that we consider are assumed to be "intrinsically straight" in the sense that, if $\mathcal{R}$ is severed (at any cross-section), the resulting open rod is straight when stress-free. We therefore may imagine that $\mathcal{R}$ has been formed by taking an open rod in a straight stress-free configuration, bringing together its ends, rotating one of the two ends in such a way that one ends up with not only $\boldsymbol{x}(L) = \boldsymbol{x}(0)$, $\boldsymbol{t}(L) = \boldsymbol{t}(0)$, but also $\boldsymbol{d}(L) = \boldsymbol{d}(0)$, and then sealing the ends.

The choice of the vectors $\boldsymbol{d}_{\mathrm{u}}(s)$ depends on the nature of the three-dimensional object being modeled or approximated by the rod. Two cases are of particular importance:

(I) In theories of intrinsically straight rods formed from materially uniform isotropic or transversely isotropic materials, if $\mathcal{R}$ is open one may choose the vectors $\boldsymbol{d}_{\mathrm{u}}(s)$ so that in a stress-free configuration (where $\Omega = \Omega_{\mathrm{u}}$) they are independent of s,** and hence such that $\Omega_{\mathrm{u}}(s) \equiv 0$. When $\mathcal{R}$ is closed, however, the choice of $\boldsymbol{d}_{\mathrm{u}}(\cdot)$ must be such that $\boldsymbol{d}(\cdot)$ is continuous in each configuration, which requires that $\boldsymbol{d}(L) = \boldsymbol{d}(0)$ and generally does not yield $\Omega_{\mathrm{u}}(s) = 0$.

(II) When $\mathcal{R}$ serves as a model for a DNA molecule, it is standard practice to identify $\mathcal{C}$ with the duplex axis; $\boldsymbol{d}(s)$ is then taken to be a unit vector perpendicular to $\mathcal{C}$ that points from $\mathcal{C}$ to the sugar-phosphate backbone of a chosen one of the two DNA strands, and $\Omega_{\mathrm{u}} = \boldsymbol{d}_{\mathrm{u}} \times \boldsymbol{d}_{\mathrm{u}}' \cdot \boldsymbol{t}_{\mathrm{u}}$ is again not zero. As Ω_{u} depends on the nucleotide sequence, it is not strictly constant in s; in theories such as the present it is identified with its average value.

The *total twist* $\mathcal{T}$ and *total excess twist* $\Delta\mathcal{T}$ (measured in turns) are

$$\mathcal{T} = \mathcal{T}(\Omega(\cdot)) = \frac{1}{2\pi} \int_0^L \Omega(s)\, \mathrm{d}s, \tag{1.2}$$

* For a modern discussion see [7].

** I.e., parallel, like the teeth of an undeformed comb.

$$\Delta\mathcal{T} = \mathcal{T}(\Omega(\cdot)) - \mathcal{T}(\Omega_{\mathrm{u}}(\cdot)) = \frac{1}{2\pi}\int_0^L \Delta\Omega(s)\,\mathrm{d}s; \tag{1.3}$$

$\Delta\Omega(\cdot) = \Omega(\cdot) - \Omega_{\mathrm{u}}(\cdot)$ is called the *density of excess twist*. In the present theory the configuration of $\mathcal{R}$ is specified when the pair $(\boldsymbol{x}(\cdot), \Delta\Omega(\cdot))$, i.e., $(\mathcal{C}, \Delta\Omega)$, is given.

Knowledge of the configuration determines the elastic energy Ψ. In the present theory, Ψ is the sum of the bending energy Ψ_{B} and the twisting energy Ψ_{T}, i.e.,

$$\Psi = \Psi_{\mathrm{B}}(\mathcal{C}) + \Psi_{\mathrm{T}}(\Delta\Omega(\cdot)), \tag{1.4}$$

where,

$$\Psi_{\mathrm{B}}(\mathcal{C}) = \frac{A}{2}\int_0^L \kappa(s)^2\,\mathrm{d}s, \tag{1.5}$$

and

$$\Psi_{\mathrm{T}}(\Delta\Omega(\cdot)) = \frac{C}{2}\int_0^L \Delta\Omega(s)^2\,\mathrm{d}s; \tag{1.6}$$

$\kappa(s) = |\boldsymbol{x}''(s)|$ is the curvature of $\mathcal{C}$; A and C are material constants called the *coefficients of flexural and torsional rigidity*. As $\mathcal{R}$ is here assumed to be impenetrable and to have circular cross-sections with diameter D, the numbers

$$\omega = C/A, \qquad d = D/L \tag{1.7}$$

are important dimensionless parameters in our theory.

Associated with each closed rod $\mathcal{R}$ is a topological parameter called the *excess link* and denoted by $\Delta\mathcal{L}$. To define $\Delta\mathcal{L}$ we first note that the *linking number* $\mathcal{L}$ of $\mathcal{R}$ is the Gauss linking number for two closed curves,[⋆] one of which is $\mathcal{C}$ and the other is the curve $\mathcal{C}^{\#}$ with points $\boldsymbol{x}^{\#} = \boldsymbol{x}(s) + \varepsilon\boldsymbol{d}(s)$, $0 \leqslant s \leqslant L$. (Here ε is a positive constant less than $D/2$.) The integer $\mathcal{L}$ is equal to the algebraic sum of the signed crossings that either one of the two curves makes with a spherical cap spanning the other. It follows that

$$\mathcal{L} = \frac{1}{4\pi}\int_{\mathcal{C}}\int_{\mathcal{C}^{\#}} \frac{\boldsymbol{t}(s)\times\boldsymbol{t}^{\#}(s^{\#})\cdot[\boldsymbol{x}(s)-\boldsymbol{x}^{\#}(s^{\#})]}{|\boldsymbol{x}(s)-\boldsymbol{x}^{\#}(s^{\#})|^3}\,\mathrm{d}s^{\#}\mathrm{d}s, \tag{1.8}$$

where $s^{\#}$ is the arc-length parameter for $\mathcal{C}^{\#}$. The linking number is invariant in all homotopic deformations of a closed impenetrable rod; i.e., $\mathcal{L}$ is a topological property of $\mathcal{R}$. The *writhe* $\mathcal{W}$ of the axial curve $\mathcal{C}$ (occasionally referred to as the "writhe of $\mathcal{R}$") is given by a double integral over $\mathcal{C}$ of the integrand with the form of that seen in (1.8):

$$\mathcal{W} = \mathcal{W}(\mathcal{C}) = \frac{1}{4\pi}\int_{\mathcal{C}}\int_{\mathcal{C}} \frac{\boldsymbol{t}(s)\times\boldsymbol{t}(\bar{s})\cdot[\boldsymbol{x}(s)-\boldsymbol{x}(\bar{s})]}{|\boldsymbol{x}(s)-\boldsymbol{x}(\bar{s})|^3}\,\mathrm{d}\bar{s}\mathrm{d}s. \tag{1.9}$$

[⋆] See, e.g., [8].

Equivalently, $\mathcal{W}$ can be defined as the average, over all orientations of a plane, of the sum of the signed self-crossings in the projection of $\mathcal{C}$ on the plane [9].* An important result of Calugareanu [11] and White [12] here implies that

$$\mathcal{L} = \mathcal{W} + \mathcal{T} \tag{1.10}$$

and tells us that although the twist and the writhe change when $\mathcal{R}$ is homotopically deformed and neither need be an integer, their sum remains fixed at an integral value. The parameter $\Delta\mathcal{L}$ is defined by the equation,

$$\Delta\mathcal{L} = \mathcal{L} - \mathcal{T}_u, \tag{1.11}$$

in which $\mathcal{T}_u = \mathcal{T}(\Omega_u(\cdot))$ is the total twist of $\mathcal{R}$ in a stress-free configuration. Thus excess link is a topological constant that need not be an integer and obeys the relation,

$$\Delta\mathcal{L} = \mathcal{W}(\mathcal{C}) + \Delta\mathcal{T}(\Delta\Omega(\cdot)), \tag{1.12}$$

in which the terms on the right are functions of the configuration of $\mathcal{R}$.

Throughout the present discussion, unless we state otherwise, we take $\mathcal{R}$ to be knot-free, i.e., we assume that $\mathcal{C}$ is topologically equivalent to a circle. For such rods equation (1.12) implies that $\Delta\mathcal{L}$ equals the excess twist $\Delta\mathcal{T}$ in any configuration in which $\mathcal{C}$ is a plane Jordan curve, such as that for which $\mathcal{C}$ is a circle.

When the closed rod $\mathcal{R}$ with circular cross-section is made from a transversely isotropic material, one can change $\Delta\mathcal{L}$ by cutting $\mathcal{R}$ at one cross-section while holding $\mathcal{C}$ fixed, adjusting $\Delta\mathcal{T}$ to the appropriate value (by rotating the cross-section on one side of the cut relative to that on the other side), and then resealing the cut. The resulting change in $\Delta\mathcal{L}$ is equal to the change in $\Delta\mathcal{T}$ (in turns). Each time $\Delta\mathcal{L}$ is changed in this way, the function $\boldsymbol{d}_u(\cdot)$ must be chosen anew in order that $\boldsymbol{d}(\cdot)$ have the required continuity properties in each configuration.**

As we have mentioned, for a DNA plasmid there is a natural choice for $\boldsymbol{d}_u$. Moreover, when a plasmid is cut it cannot be resealed unless the cross-sections at the cut are joined without rotation or after rotation through an integral number of turns. Nonetheless, as $\mathcal{T}_u$ for DNA depends on the chemical composition and temperature of the solvent (and is far more sensitive to those variables than are the elastic constants A and C), one can design experiments in which $\Delta\mathcal{L}$ is varied continuously over a broad range.

In this paper we shall present bifurcation diagrams for equilibrium configurations as graphs of excess link, $\Delta\mathcal{L}$, versus writhe, $\mathcal{W}$. Results that are given in [1, 2] and here in Section 3 show that such diagrams contain useful information

* An elementary exposition of the theory of linking number and writhe and its applications in molecular biology has been given by White [10].

** It is interesting to note that, although both the values of $\mathcal{L}$ and Ω_u after the cut is resealed depend on the choice made for the function $\boldsymbol{d}_u(\cdot)$, the excess link does not depend on $\boldsymbol{d}_u(\cdot)$.

about the stability of calculated configurations. The stability criteria we employ refer to virtual processes in which $\Delta\mathcal{L}$ is changed continuously with the elastic coefficients A and C held fixed.

Throughout the present discussion it is assumed that the only external forces that act on $\mathcal{R}$ are those that can be attributed to contact of $\mathcal{R}$ with itself.[⋆] It therefore follows from Kirchhoff's form of the equations of balance of linear and angular momentum that in a state of mechanical equilibrium, at values of s other than those characterizing points of self-contact,[⋆⋆] there holds

$$\boldsymbol{F}' = \boldsymbol{0}, \qquad \boldsymbol{M}' = \boldsymbol{F} \times \boldsymbol{t}, \tag{1.13}$$

where $\boldsymbol{F} = \boldsymbol{F}(s)$ and $\boldsymbol{M} = \boldsymbol{M}(s)$ are the internal force and moment acting on the cross-section at s.[‡] It is a consequence of the relations (1.4)–(1.6) for Ψ that $\boldsymbol{M}$ obeys the constitutive equation

$$\boldsymbol{M} = A\boldsymbol{t} \times \boldsymbol{t}' + C\Delta\Omega\boldsymbol{t}; \tag{1.14}$$

$\boldsymbol{F}$ is a reactive force not given by a constitutive relation.

We confine attention to cases in which self-contact, when it occurs, is such that the boundary of a given cross-section is in contact with the boundary of at most one other. In our present subject, a *point of self-contact* is a (single) point in space at which the boundaries of two cross-sections meet. We assume that the forces the two cross-sections exert on each other are reactive forces normal to the surface of $\mathcal{R}$. If we let s^* and s^{**} (with $s^{**} \neq s^*$) be the arc-length parameters for the two cross-sections in contact, geometrical considerations give us the relations,

$$|\boldsymbol{x}(s^*) - \boldsymbol{x}(s^{**})| = D, \tag{1.15}$$

$$\boldsymbol{t}(s^*) \cdot [\boldsymbol{x}(s^*) - \boldsymbol{x}(s^{**})] = 0. \tag{1.16}$$

Under our present hypotheses the set of points of self-contact is a union of N isolated points and J spatial curves called *contact curves*.

When s^* corresponds to an isolated point of self-contact or an endpoint of a contact curve, the contact force at s^* is a concentrated force $\boldsymbol{f}^*$, and

$$[\boldsymbol{F}](s^*) + \boldsymbol{f}^* = \boldsymbol{0}, \qquad [\boldsymbol{M}](s^*) = \boldsymbol{0}, \tag{1.17}$$

where $[\boldsymbol{F}](s^*) = \lim_{s\to s^*+} \boldsymbol{F}(s) - \lim_{s\to s^*-} \boldsymbol{F}(s)$, etc.

For each of the two subsegments of $\mathcal{R}$ that meet at a contact curve, the range of the arc-length coordinate is, of course, an interval. Throughout the interior $\hat{\mathcal{J}}$ of

⋆ A more general case is discussed in [1].

⋆⋆ Which are those where a point on the surface of $\mathcal{R}$ touches another point on the surface and hence the two become one point in space.

‡ More precisely, $\boldsymbol{F}(\bar{s})$ is the resultant of the Piola stresses exerted on the cross-section at $s = \bar{s}$ by the material on the side where $s > \bar{s}$, and $\boldsymbol{M}(\bar{s})$ is the resultant of the moments (about the point $\boldsymbol{x}(\bar{s})$) of those Piola stresses.

that interval the contact force has a continuous density $\boldsymbol{f}(\cdot)$, both $\boldsymbol{F}(\cdot)$ and $\boldsymbol{M}(\cdot)$ are smooth functions, and

$$\boldsymbol{F}'(s^*) + \boldsymbol{f}(s^*) = \boldsymbol{0}, \qquad \boldsymbol{M}'(s^*) = \boldsymbol{F}(s^*) \times \boldsymbol{t}(s^*), \quad \text{for } s^* \text{ in } \hat{\mathcal{J}}. \tag{1.18}$$

As we here assume that the contact forces are shear-free, regardless of whether these forces are concentrated or have a density,

$$\boldsymbol{f}(s^*) = -\boldsymbol{f}(s^{**}) = f(s^*)\frac{\boldsymbol{x}(s^*) - \boldsymbol{x}(s^{**})}{D}. \tag{1.19}$$

In both cases the function $\boldsymbol{M}(\cdot)$ is continuous.

The assumptions we have made imply that wherever either (1.13) or (1.18) holds, i.e., wherever the contact force vanishes or has a continuous density, $(\boldsymbol{M} \cdot \boldsymbol{t})' = \boldsymbol{M} \cdot \boldsymbol{t}' = 0$ and, by (1.14), $\Delta\Omega' = 0$. As $\boldsymbol{M}(\cdot)$ is continuous (even at the isolated values of s where $\boldsymbol{f}$ is a concentrated force), we may conclude that, under our present assumptions about the nature of forces of self-contact, in an equilibrium configuration the excess twist density $\Delta\Omega$ equals the constant $2\pi\,\Delta\mathcal{T}/L$.

The problem of characterizing the equilibrium configurations of a rod subject to appropriate boundary conditions and topological constraints is one of finding pairs $(\mathcal{C}, \Delta\Omega)$ that obey the *equations of mechanical equilibrium* (1.13)–(1.19). We are here concerned with the solutions of those equations for which $\boldsymbol{x}(\cdot)$ is of class C^3 at all but a finite number of values of s.[⋆] For closed rods we impose the constraints that $\Delta\mathcal{L}$ and the knot-type of $\mathcal{C}$ have their preassigned values and that

$$\boldsymbol{x}^{(n)}(0) = \boldsymbol{x}^{(n)}(L) \quad (n = 0, 1, 2, 3), \tag{1.20}$$

where $\boldsymbol{x}^{(0)} = \boldsymbol{x}$, $\boldsymbol{x}^{(1)} = \boldsymbol{x}'$, etc. For the calculations reported in this paper, the point $s = 0$ is chosen so that it does not characterize a point of self-contact for $\mathcal{R}$.

A pair $(\mathcal{C}, \Delta\Omega)$, whether or not it is a solution of the equations (1.13)–(1.20), is "physically acceptable" and can be called a configuration of $\mathcal{R}$ only if it obeys a condition expressing our assumption that $\mathcal{R}$ is impenetrable:[⋆⋆]

Condition Γ. If two distinct cross-sections of $\mathcal{R}$ have a point in common, that point is on the boundaries of the two cross-sections.

Let $\delta(s, \bar{s})$ be the Euclidean distance between the points of $\mathcal{C}$ with arc-length parameters s and $\bar{s}$, and let $\Delta(s)$ be the smallest of the non-zero stationary values of $\delta(s, \bar{s})$ as $\bar{s}$ varies over $\mathcal{C}$:

$$\delta(s, \bar{s}) = |\boldsymbol{x}(s) - \boldsymbol{x}(\bar{s})|, \tag{1.21}$$

$$\Delta(s) = \min_{0 \leqslant \bar{s} < L} \{\delta(s, \bar{s}) \mid \mathrm{d}\delta(s, \bar{s})/\mathrm{d}\bar{s} = 0,\ \bar{s} \neq s\}. \tag{1.22}$$

⋆ In the present theory of equilibrium configurations, $\boldsymbol{t}(\cdot)$ and $\boldsymbol{t}'(\cdot)$ are continuous functions, $\boldsymbol{t}''(\cdot)$ has jump discontinuities only at values of s characterizing isolated points of self-contact or extreme points of intervals of self-contact; at such points, $\boldsymbol{b}(\cdot)$ is continuous (provided $\kappa \neq 0$) but κ' and τ may suffer jump discontinuities. As we have seen, $\Delta\Omega(\cdot)$ is constant throughout $\mathcal{R}$.

⋆⋆ Of course, a configuration $(\mathcal{C}, \Delta\Omega)$ must also obey the closure conditions.

In calculations of equilibrium configurations $(\mathcal{C}, \Delta\Omega)$ we have found it useful to make use of the fact that, in order for $\mathcal{C}$ to obey condition Γ, it is necessary and sufficient that*

$$\min_{0 \leqslant s < L} \{2\kappa^{-1}(s), \Delta(s)\} \geqslant D. \tag{1.23}$$

An important property of a configuration is its *contact diagram*. In the language of graph theory, such a diagram is a graph for which each vertex represents either an isolated point of self-contact or an endpoint of a contact curve. The vertices are connected by edges of two types, called *simple* and *double edges*, according to the following rules: (i) Each simple edge represents a unique, maximal, contact-free subsegment of $\mathcal{R}$.** (ii) Each double edge represents a (unique) contact curve or, equivalently, a pair of subsegments that are in contact along their lengths.

The contact diagram of a configuration of $\mathcal{R}$ has the topology of a body (in 3-space) obtained by gluing together each pair of material points of $\mathcal{R}$ that correspond to a single point of self-contact. Figure 1 contains all the contact diagrams appropriate to the equilibrium configurations discussed in this paper. Whenever a configuration will be shown, its contact diagram will be indicated in the notation of Figure 1.

It can happen that one value of $\Delta\mathcal{L}$ can give rise to two or more equilibrium configurations with different values of N and J, or, as shown in Figure 2, the same values of N and J but with different contact diagrams.

In the next section we present explicit solutions of equations (1.13)–(1.20), the equations obeyed by a closed rod that is in mechanical equilibrium. We there give a detailed discussion of our method of determining the dependence of integration constants on ω, d, and $\Delta\mathcal{L}$.

2. Solution of the Equilibrium Equations

The equations (1.13), with $\boldsymbol{M}$ as in (1.14), are obeyed by each subsegment of $\mathcal{R}$ that is free from points at which $\mathcal{R}$ makes contact with itself. The observation that (1.13) and (1.14) together are equivalent to Euler's equations for the motion of a symmetric top has been called "Kirchhoff's top analogy". When the analogy is employed, s is interpreted as time, $\boldsymbol{d}$ as a unit vector imbedded in the top and perpendicular to its axis of symmetry, $\boldsymbol{t}$ as a unit vector with the direction of that axis, and $\boldsymbol{F}$ as the resultant of the gravitational force on the top. Familiar results in the theory of tops yield explicit expressions for the Euler angles describing the orientation of the triad $(\boldsymbol{t}, \boldsymbol{d}, \boldsymbol{t} \times \boldsymbol{d})$ as a function of s, a fact employed by Le Bret [14] to calculate contact-free configurations of plasmids. Several writers, the earliest that we know of being Landau and Lifshitz [15], have remarked that use of a particular cylindrical coordinate system simplifies the problem of obtaining

* Cf. [13].

** Simple loops, i.e., simple edges that connect a vertex to itself, not only occur, but are common in knot-free plasmids.

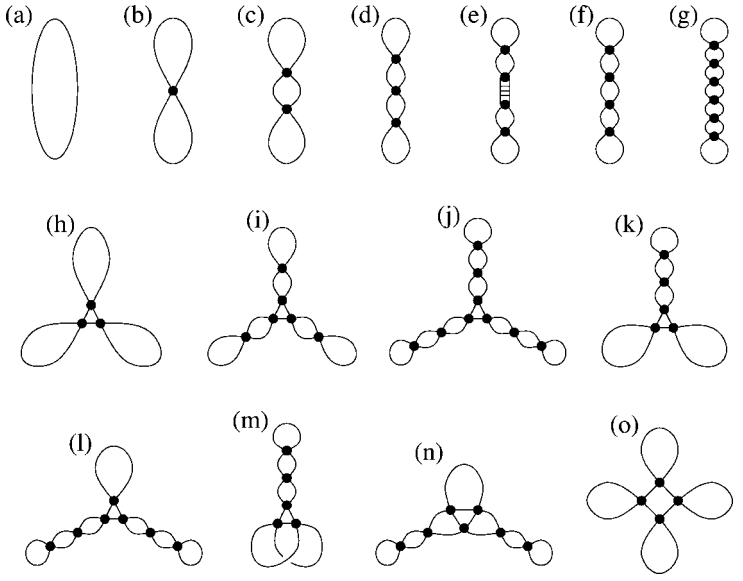

Figure 1. Selected contact diagrams for equilibrium configurations of a knot-free closed rod. Each vertex (solid circle) corresponds to an isolated point of self-contact or an end point of a contact curve. The simple edges (solid curves) correspond to contact free subsegments. Diagram (e) contains a double edge (shown as a three-step "ladder") that corresponds to a contact curve.

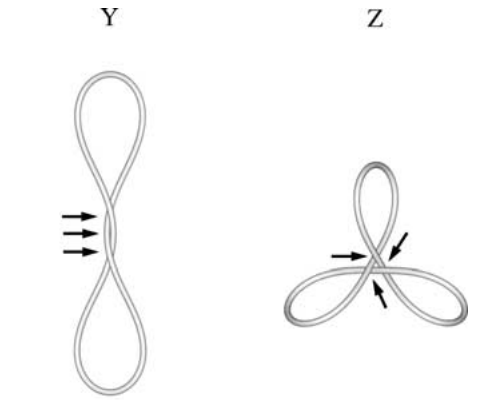

Figure 2. Two distinct equilibrium configurations with $d = 8.2 \times 10^{-3}$, $\omega = 2/3$, $\Delta\mathcal{L} = 2.5$, $N = 3$, $J = 0$. Points of self-contact are marked with arrows. Labels give the corresponding excess link $\Delta\mathcal{L}$, writhe $\mathcal{W}$, and contact diagram (δ).

an explicit expression for the axial curve. The expression contains six integration constants, here called *solution parameters*, which determine the configuration to within a translation and rotation of $\mathcal{C}$. We employ that coordinate system here and a method of calculating the solution parameters [16] that is useful when such constraints as end-conditions and $\Delta\mathcal{L}$ are specified (cf. [17, 18]).

CONFIGURATIONS WITH ONLY ISOLATED POINTS OF SELF-CONTACT

At each of the N spatial points at which an isolated point of self-contact occurs, two material points on the surface of the rod come together. For each i, $i = 1, 2, \ldots, 2N$, we let s_i, with $0 < s_1 < s_2 < \cdots < s_{2N} < L$, be the arc-length parameter of a cross-section that is in contact with another cross-section in this way. In addition, we put $s_0 = 0$ and $s_{2N+1} = L$. If, for $i = 1, 2, ..., 2N + 1$, we let $\mathcal{R}_i$, with axial curve $\mathcal{C}_i$, be the subsegment of $\mathcal{R}$ that is bounded by the cross-sections at s_{i-1} and s_i, we obtain a decomposition of $\mathcal{R}$ into $2N + 1$ subsegments, on each of which (1.13) holds in the interior of the corresponding axial curve.*

For the $2N - 1$ subsegments $\mathcal{R}_i$ with $2 \leqslant i \leqslant 2N$ the boundary conditions imposed at the two end-points of $\mathcal{C}_i$ are governed by the equations (1.15)–(1.17) and (1.19) in which the pairs (s^*, s^{**}) and the vectors $\boldsymbol{f}^*$ are parameters that depend on i and are to be determined from the constraints on $\mathcal{R}$. For the remaining two subsegments, $\mathcal{R}_1$ and $\mathcal{R}_{2N+1}$, the end-conditions at one end are governed by (1.15)–(1.17) and (1.19), and at the other (where $s = 0$ or L) by the relations (1.20).**

As the first equation of the pair (1.13) asserts that $\boldsymbol{F}$ is equal to a constant vector $\boldsymbol{F}_i$ for $s_{i-1} < s < s_i$, we may integrate the second equation to obtain the relation,

$$\boldsymbol{M} = \boldsymbol{F}_i \times \boldsymbol{r} + \boldsymbol{M}_i^0, \tag{2.1}$$

in which $\boldsymbol{r} = \boldsymbol{x} - \boldsymbol{x}_i^0$ and $\boldsymbol{M}_i^0$ is a constant that depends on the choice of the origin $\boldsymbol{x}_i^0$. As in [16–18], we choose $\boldsymbol{x}_i^0$ so that $\boldsymbol{M}_i^0$ is parallel to $\boldsymbol{F}_i$.

The number T_i, defined by

$$T_i = \omega\sqrt{\frac{2A}{F_i}}\Delta\Omega, \quad F_i = |\boldsymbol{F}_i|, \tag{2.2}$$

serves as a dimensionless measure of the density of excess twist in the i-th segment.‡ When describing solutions of (1.13) in that segment, we henceforth shall

* When $\mathcal{R}$ is free from self-contact, $N = 1$, $\mathcal{R}_i = \mathcal{R}_1 = \mathcal{R}$, and the present theory reduces to one presented in previous articles [16–18].

** We have deliberately employed a subdivision of the closed rod insuring that s_0 and s_{2N+1} do not characterize contact points but instead correspond to a single point in the interior of an interval of $\mathcal{C}$ on which (1.13) has a classical solution with $\boldsymbol{x}(\cdot)$ of class C^3.

‡ In writing (2.2) we make use of the fact that in equilibrium $\Delta\Omega$ is independent of both s and i.

use $\sqrt{2A/F_i}$ as the unit of length and thus render s and $\boldsymbol{r}$ dimensionless. When this is done, the relations (1.14) and (2.1) yield

$$\boldsymbol{r}' \times \boldsymbol{r}'' + T_i \boldsymbol{r}' = 2[\boldsymbol{k}_i \times \boldsymbol{r} + \lambda_i \boldsymbol{k}_i], \tag{2.3}$$

where λ_i, like T_i, is a constant and $\boldsymbol{k}_i$ is a unit vector parallel to $\boldsymbol{F}_i$.

We employ a Cartesian system such that (i) its origin is at $\boldsymbol{x}_i^0$, (ii) its x-axis contains a point on $\mathcal{C}_i$ (or, as explained below after equation (2.18), an appropriate extension of $\mathcal{C}_i$) at which the curvature κ attains its maximum value, and (iii) the vector $\boldsymbol{k}_i$ in (2.3) gives the direction of increasing z; the relations

$$x = r\cos\phi, \qquad y = r\sin\phi, \tag{2.4}$$

then define associated cylindrical coordinates (r, ϕ, z). It is not difficult to show that equation (2.3) implies that such Cartesian systems exist and that $\kappa(\cdot)$ and $r(\cdot)$ are bounded.

For each choice of the dimensionless parameters T_i and λ_i, (2.3) is a system of three differential equations that one can solve to obtain the function $\boldsymbol{r}(\cdot)$. To this end we note that in our cylindrical coordinate system the condition of inextensibility, $(x')^2 + (y')^2 + (z')^2 = 1$, becomes

$$(r')^2 = 1 - u(\phi')^2 - (z')^2, \quad u = r^2. \tag{2.5}$$

The component along $\boldsymbol{t}$ of the vector product of equation (2.3) with $\boldsymbol{k}_i$ reduces to $z'' = -u'$ which yields

$$z' = a_i - u, \tag{2.6}$$

with a_i another constant of integration. From (2.3), (2.4), and (2.6) we obtain

$$\phi' = u^{-1}\left[\frac{T_i}{2} - \lambda_i(a_i - u)\right]. \tag{2.7}$$

The three equations (2.5), (2.6), (2.7) have the following explicit solution [16]:

$$r^2 = u_{3,i} - (u_{3,i} - u_{2,i})\sin^2\psi, \tag{2.8}$$

$$\phi = \lambda_i(s - s_i^0) + \frac{[(T_i/2) - \lambda_i a_i]\Pi(n_i; \psi \mid m_i)}{u_{3,i}\sqrt{u_{3,i} - u_{1,i}}}, \tag{2.9}$$

$$z = (a_i - u_{1,i})(s - s_i^0) - \sqrt{u_{3,i} - u_{1,i}}\,\mathrm{E}(\psi \mid m_i); \tag{2.10}$$

here

$$\sin\psi = \mathrm{sn}\big((s - s_i^0)\sqrt{u_{3,i} - u_{1,i}}\big), \quad \text{i.e.,} \quad s - s_i^0 = \mp\frac{\mathrm{F}(\psi \mid m_i)}{\sqrt{u_{3,i} - u_{1,i}}}, \tag{2.11}$$

$$m_i = (u_{3,i} - u_{2,i})/(u_{3,i} - u_{1,i}), \qquad n_i = (u_{3,i} - u_{2,i})/u_{3,i}, \tag{2.12}$$

and $u_{1,i}$, $u_{2,i}$, and $u_{3,i}$, with $u_{1,i} \leqslant 0 \leqslant u_{2,i} \leqslant u_{3,i}$, are the roots of the cubic polynomial

$$\begin{aligned} P_i(u) &= -[u^3 + (\lambda_i^2 - 2a_i)u^2 + (a_i^2 - 2a_i\lambda_i^2 + T_i\lambda_i - 1)u \\ &\quad + (\tfrac{1}{2}T_i - a_i\lambda_i)^2] \\ &= (u - u_{1,i})(u - u_{2,i})(u_{3,i} - u). \end{aligned} \tag{2.13}$$

In (2.8)–(2.10), sn is a Jacobi elliptic function with parameter m_i, and F, E, Π are the elliptic integrals,

$$\mathrm{F}(\psi \mid m) = \int_0^{\psi} \frac{\mathrm{d}\zeta}{\sqrt{1 - m\sin^2\zeta}}, \tag{2.14}$$

$$\mathrm{E}(\psi \mid m) = \int_0^{\psi} \sqrt{1 - m\sin^2\zeta}\,\mathrm{d}\zeta, \tag{2.15}$$

$$\Pi(n; \psi \mid m) = \int_0^{\psi} \frac{\mathrm{d}\zeta}{(1 - n\sin^2\zeta)\sqrt{1 - m\sin^2\zeta}}. \tag{2.16}$$

It follows from (2.3) that τ, the geometric torsion of $\mathcal{C}$, is an affine function of κ^{-2} (cf. [19]), i.e.,

$$\tau = \tfrac{1}{2}T_i - [4\lambda_i + \tfrac{1}{2}T_i^3 - 2T_i(\lambda_i^2 + a_i)]\kappa^{-2} \tag{2.17}$$

and that κ^2 is an affine function of r^2 [16]:

$$\kappa^2 = 4(r^2 + \lambda_i^2) - T_i^2; \tag{2.18}$$

here τ and κ are in our present dimensionless units.

The value s_i^0 of s that appears in (2.9)–(2.11) does not always lie in the interval $s_{i-1} < s < s_i$. It is chosen so that, on the extension of the solution (2.8)–(2.10) of (2.5)–(2.7) from $s_{i-1} < s < s_i$ to $(-\infty, \infty)$, the maximum value of $\kappa(s)$ (and hence of $r(s)$) is attained at s_i^0.

The dimensionless parameters a_i, λ_i, T_i determine the roots $u_{1,i}$, $u_{2,i}$, $u_{3,i}$ of the polynomial P_i and hence the coordinates r, ϕ, z as functions $r(\cdot)$, $\phi(\cdot)$, $z(\cdot)$ of $s - s_i^0$. Specification of the configuration $(\mathcal{C}_i, \Delta\Omega)$ of the subsegment $\mathcal{R}$ requires knowledge of the endpoints,

$$\sigma_i^- = s_{i-1} - s_i^0, \qquad \sigma_i^+ = s_i - s_i^0, \tag{2.19}$$

of the interval serving as the domain for $r(\cdot)$, $\phi(\cdot)$, $z(\cdot)$, and also of the scale factor, $\sqrt{2A/F_i}$, or, equivalently, of the length L_i of $\mathcal{R}_i$ in conventional (as opposed to dimensionless) units:

$$L_i = \sqrt{2A/F_i}(s_i - s_{i-1}). \tag{2.20}$$

It is not difficult to verify that the sextuple $(a_i, \lambda_i, T_i, \sigma_i^-, \sigma_i^+, L_i)$ of solution parameters determines the pair $(\mathcal{C}_i, \Delta\Omega)$ to within a rigid rotation and translation of $\mathcal{C}_i$.

Moreover, one can show (see [17]) that for each subsegment $\mathcal{R}_i$ the elastic energies Ψ^i, Ψ^i_{B}, and Ψ^i_{T} (in conventional units, e.g., ergs) are given by the relations,

$$\Psi^i = \frac{2A(\sigma_i^+ - \sigma_i^-)^2}{L_i}\left[a_i + \lambda_i^2 - \zeta_i + \tfrac{1}{4}(\omega^{-1} - 1)T_i^2\right], \tag{2.21}$$

$$\Psi^i_{\mathrm{B}} = \frac{2A(\sigma_i^+ - \sigma_i^-)^2}{L_i}\left[a_i + \lambda_i^2 - \zeta_i - \tfrac{1}{4}T_i^2\right], \tag{2.22}$$

$$\Psi^i_{\mathrm{T}} = \frac{A(\sigma_i^+ - \sigma_i^-)^2 T_i^2}{2\omega L_i}, \tag{2.23}$$

where ζ_i is the ratio of the difference in z-coordinates of the end points of the segment to its length:

$$\zeta_i = [z(\sigma_i^+) - z(\sigma_i^-)]/(\sigma_i^+ - \sigma_i^-). \tag{2.24}$$

Let $(\boldsymbol{t}_i, \boldsymbol{n}_i, \boldsymbol{b}_i) = (\boldsymbol{t}(s_i), \boldsymbol{n}(s_i), \boldsymbol{b}(s_i))$, with $\boldsymbol{n} = \boldsymbol{t}'/\kappa$ and $\boldsymbol{b} = \boldsymbol{t} \times \boldsymbol{n}$, be the Serret–Frenet triad at s_i, and let $\boldsymbol{Q}_i$ be the orthogonal tensor such that

$$\boldsymbol{Q}_i \boldsymbol{t}_{i-1} = \boldsymbol{t}_i, \qquad \boldsymbol{Q}_i \boldsymbol{n}_{i-1} = \boldsymbol{n}_i, \qquad \boldsymbol{Q}_i \boldsymbol{b}_{i-1} = \boldsymbol{b}_i. \tag{2.25}$$

Once the solution parameters $(a_i, \lambda_i, T_i, \sigma_i^-, \sigma_i^+, L_i)$ are specified, the equations (2.4) and (2.6) yield (by differentiation) explicit expressions for the triad $(\boldsymbol{t}(\cdot), \boldsymbol{n}(\cdot), \boldsymbol{b}(\cdot))$, and one knows the tensor $\boldsymbol{Q}_i$ and also the components (h_i^t, h_i^n, h_i^b) and (F_i^t, F_i^n, F_i^b) of the vectors $\boldsymbol{h}_i = \boldsymbol{x}(s_i) - \boldsymbol{x}(s_{i-1})$ and $\boldsymbol{F}_i$ with respect to the basis $(\boldsymbol{t}_{i-1}, \boldsymbol{n}_{i-1}, \boldsymbol{b}_{i-1})$.

It follows from (1.14), the continuity of $\boldsymbol{t}(\cdot)$, and the relation $[\boldsymbol{M}](s_i) = \boldsymbol{0}$ (see (1.17)), that $\boldsymbol{b}(\cdot)$, $\boldsymbol{n}(\cdot)$, and $\kappa(\cdot)$ are continuous on all of $\mathcal{C}$ except possibly a finite number of points where $\boldsymbol{n}(\cdot)$ and $\boldsymbol{b}(\cdot)$ have jump discontinuities (which can happen only where $\kappa = 0$). If we suppose that κ is not zero at any of the points s_i, then

$$\boldsymbol{t}_j = \boldsymbol{Q}_j \boldsymbol{Q}_{j-1} \cdots \boldsymbol{Q}_{i+1} \boldsymbol{t}_i, \quad \text{for } 0 \leqslant i < j \leqslant 2N+1, \tag{2.26}$$

and this relation holds also with $\boldsymbol{t}$ replaced by $\boldsymbol{n}$ and $\boldsymbol{b}$. It follows that

$$\begin{aligned}
&\boldsymbol{x}(s_j) - \boldsymbol{x}(s_i) \\
&\quad = \sum_{k=i+1}^{j} \boldsymbol{h}_k = (h_{i+1}^t + h_{i+2}^t \boldsymbol{Q}_{i+1} + \cdots + h_j^t \boldsymbol{Q}_{j-1} \boldsymbol{Q}_{j-2} \cdots \boldsymbol{Q}_{i+1})\boldsymbol{t}_i \\
&\qquad\qquad + (h_{i+1}^n + h_{i+2}^n \boldsymbol{Q}_{i+1} + \cdots + h_j^n \boldsymbol{Q}_{j-1} \boldsymbol{Q}_{j-2} \cdots \boldsymbol{Q}_{i+1})\boldsymbol{n}_i \\
&\qquad\qquad + (h_{i+1}^b + h_{i+2}^b \boldsymbol{Q}_{i+1} + \cdots \\
&\qquad\qquad + h_j^b \boldsymbol{Q}_{j-1} \boldsymbol{Q}_{j-2} \cdots \boldsymbol{Q}_{i+1})\boldsymbol{b}_i
\end{aligned} \tag{2.27}$$

and

$$\begin{aligned}
[\boldsymbol{F}](s_i) = \boldsymbol{F}_{i+1} - \boldsymbol{F}_i \;=\; &(F_{i+1}^t - F_i^t \boldsymbol{Q}_i^{-1})\boldsymbol{t}_i + (F_{i+1}^n - F_i^n \boldsymbol{Q}_i^{-1})\boldsymbol{n}_i \\
&+ (F_{i+1}^b - F_i^b \boldsymbol{Q}_i^{-1})\boldsymbol{b}_i,
\end{aligned} \tag{2.28}$$

where $\boldsymbol{F}_i$ equals the (constant) value of $\boldsymbol{F}$ in the open interval $s_{i-1} < s < s_i$.

We are supposing here that values have been assigned in advance to the parameters D, L, ω, and also to $\Delta\mathcal{L}$. Once one knows (or has assumed) that $\mathcal{R}$ has a particular contact diagram (and hence a particular value of N), one knows the pairs (i, j) of indexes associated with the arc-length parameters (s_i, s_j) of the pairs of cross-sections that are in contact, and one can construct a system $\mathcal{E}$ of $12N + 6$ nonlinear algebraic equations for the $12N + 6$ members of the parameter set

$$\mathcal{Q} = \{(a_i, \lambda_i, T_i, \sigma_i^-, \sigma_i^+, L_i) \mid i = 1, 2, \ldots, 2N + 1\} \tag{2.29}$$

in such a way that a solution of $\mathcal{E}$ (if one can be found) yields, when inserted into the equations (2.8)–(2.10), a pair $(\mathcal{C}, \Delta\Omega)$ that obeys: (i) the differential equations (2.5)–(2.7), (ii) the closure conditions (1.20), (iii) the geometrical relations (1.15) and (1.16), (iv) the jump conditions (1.17) with contact forces as in (1.19), (v) the equations (2.2) (in which $\Delta\Omega$ is independent of i), (vi) the obvious requirement that

$$\sum_{i=1}^{2N+1} L_i = L, \tag{2.30}$$

and (vii) the requirement that $\mathcal{W}(\mathcal{C}) + \Delta\Omega L/2\pi$ be equal to the preassigned value of $\Delta\mathcal{L}$.*

In the search for a solution of the algebraic system $\mathcal{E}$ one can employ a Newton–Raphson iterative algorithm that converges quadratically when a good initial guess is made for $\mathcal{Q}$. When, as here, one is concerned with families of equilibrium configurations with varying $\Delta\mathcal{L}$, one may advance along such a family by a procedure in which the initial guess in the search for the set $\mathcal{Q}_\#$ corresponding to a value $\Delta\mathcal{L}_\#$ of $\Delta\mathcal{L}$, is a set $\mathcal{Q}_0$ that is known to correspond to a value of $\Delta\mathcal{L}$ near to $\Delta\mathcal{L}_\#$. Such a procedure may lead to difficulties at the points at which the Jacobian of $\mathcal{E}$ is singular, e.g., at turning or bifurcation points. To avoid such difficulties we employed a standard "arc-length continuation procedure" based on the observation that, by theorem of Milnor [20], the one-dimensional manifold $\mathcal{M}$ that lies in the $(12N + 6)$-dimensional space of solution parameters and corresponds to a family of equilibrium configurations with varying $\Delta\mathcal{L}$ is smooth. The procedure may be described as follows: Let $\mathcal{Q}$ be a point on $\mathcal{M}$, let $d(\mathcal{Q})$ be a vector tangent to $\mathcal{M}$ at $\mathcal{Q}$, and let $\mathcal{E}^\dagger(\mathcal{Q}, \varepsilon)$ be a system of $12N + 6$ algebraic equations obtained from $\mathcal{E}$ by first removing the equation corresponding to the requirement that $\mathcal{W} + \Delta\mathcal{T}$ have a preassigned value and then adding the equation that expresses the constraint that the solution of $\mathcal{E}^\dagger(\mathcal{Q}, \varepsilon)$ be on the hyperplane that is perpendicular to $d(\mathcal{Q})$ and passes through the point $\mathcal{Q}_\varepsilon = \mathcal{Q} + \varepsilon d(\mathcal{Q})$. To advance along $\mathcal{M}$, one starts with a known point $\mathcal{Q}$ on $\mathcal{M}$ and, for a preassigned value of the step ε, finds another such

* By using (2.26)–(2.28) to express (1.12), (1.15), (1.16), (1.17), (1.19), (1.20), (2.2), (2.30) in terms of the elements of $\mathcal{Q}$, the system $\mathcal{E}$ is cast into the form of a set of algebraic equations relating transcendental functions of those elements.

point by solving $\mathcal{E}^{\dagger}(\mathcal{Q}, \varepsilon)$ using the Newton–Raphson iterative algorithm with $\mathcal{Q}_{\varepsilon}$ the initial guess.

It may happen that a one-parameter family of pairs $(\mathcal{C}, \Delta\Omega)$ generated in this manner contains pairs that do not meet the requirement that condition Γ hold. As we shall see in Section 4, a family containing such pairs can connect one set of physically acceptable pairs to another and hence explain the occurrence of isolas in a bifurcation diagram. (See also [21] and the discussion in the footnote $\star$ on page 210.)

The calculation that yields the curve $\mathcal{C}$ and the excess twist density $\Delta\Omega$ yields also (in conventional units) the arc-length parameters s_i of the contact points, the corresponding contact forces $\boldsymbol{f}(s_i)$, and, by (2.21) and (2.22), the total elastic energy Ψ:

$$\Psi = \sum_{i=1}^{2N+1} \Psi^i = \Psi_{\mathrm{B}} + \Psi_{\mathrm{T}}, \qquad \Psi_{\mathrm{B}} = \sum_{i=1}^{2N+1} \Psi_{\mathrm{B}}^i, \qquad \Psi_{\mathrm{T}} = \frac{CL}{2}(\Delta\Omega)^2. \tag{2.31}$$

REMARK. If explicit expressions for $\boldsymbol{x}(\cdot)$ were not available, it would be difficult to evaluate the functional $\mathcal{W}(\cdot)$ needed to employ equation (1.12) to relate the pair $(\mathcal{C}, \Delta\Omega)$ to $\Delta\mathcal{L}$. However, as equations (2.8)–(2.10), (2.17), (2.18) here yield explicit formulae for $\boldsymbol{x}(\cdot)$ and $\tau(\cdot)$, we can obtain $\mathcal{W}(\mathcal{C})$ from a relation that has been discussed by Calugareanu [11], Pohl [22], and White [12]:*

$$\mathcal{W} = \mathcal{S} - \frac{1}{2\pi}\Theta, \qquad \Theta = \oint_{\mathcal{C}} \tau(s)\,\mathrm{d}s. \tag{2.32}$$

The number $\mathcal{S}$, called the *self-link* of $\mathcal{C}$, is an integer equal to the linking number of the curve $\mathcal{C}$ with the (closed) curve $\mathcal{C}_{\varepsilon}$ traced out by points on the normal vectors $\boldsymbol{n}(s)$ of $\mathcal{C}$ at a small distance ε from $\mathcal{C}$. It follows from (2.32) that $\mathcal{W}$ differs from $-\Theta/2\pi$ by an integer. Although self-link has several interesting geometric interpretations [22], no easily evaluated expression for it is known. However, if one evaluates Θ with precision and has in hand an approximate value $\mathcal{W}^{\mathrm{p}}$ for $\mathcal{W}$, the value of $\mathcal{S}$ can be obtained by rounding off $\mathcal{W}^{\mathrm{p}} + \Theta/2\pi$ to the nearest integer. A discretization yielding a value of $\mathcal{W}^{\mathrm{p}}$ sufficiently close to $\mathcal{W}$ to fix $\mathcal{S}$ is available.** For the configurations under consideration here, $\boldsymbol{n}$ is a smooth function of s for all s, and hence Θ is the sum of the torsion integrals Θ_i for the curves $\mathcal{C}_i$:‡

$$\Theta = \sum_{i=1}^{2N+1} \Theta_i, \qquad \Theta_i = \int_{\mathcal{C}_i} \tau(s)\,\mathrm{d}s. \tag{2.33}$$

* Cf. [18].

** [18], equations B2–B5.

‡ Reference [18] contains a generalization of (2.33) to cases in which a subsegment of $\mathcal{R}$ is held rigid in such a way that $\boldsymbol{n}$ suffers jumps at the endpoints of the subsegment.

Equations (2.8), (2.17), and (2.18) yield the following expression for Θ_i in terms of $(a_i, \lambda_i, T_i, \sigma_i^-, \sigma_i^+, L_i)$:

$$\Theta_i = \frac{(\sigma_i^+ - \sigma_i^-)T_i}{2} - \frac{4\lambda_i + \frac{1}{2}T_i^3 - 2(\lambda_i^2 + a_i)T_i}{[4(u_{3,i} + \lambda_i^2) - T_i^2]\sqrt{u_{3,i} - u_{1,i}}} \times \big(\Pi(\tilde{n}_i; \psi_i^+ \mid m_i) - \Pi(\tilde{n}_i; \psi_i^- \mid m_i)\big); \tag{2.34}$$

here

$$\tilde{n}_i = \frac{u_{3,i} - u_{2,i}}{u_{3,i} + \lambda_i^2 - \frac{1}{4}T_i^2}, \qquad \sigma_i^{\pm} = \frac{\mathrm{F}(\psi_i^{\pm} \mid m_i)}{\sqrt{u_{3,i} - u_{1,i}}}, \tag{2.35}$$

m_i, $u_{1,i}$, etc., are as in (2.8)–(2.13), and F and Π are as in (2.14) and (2.16).

CONFIGURATIONS WITH INTERVALS OF SELF-CONTACT

We turn now to cases in which $\mathcal{R}$ contains a pair of subsegments $\mathcal{R}^*$, $\mathcal{R}^{**}$ that meet at a contact curve. Let $\hat{\mathcal{J}}^*$ be the interior of the interval $\mathcal{J}^*$ of values of s corresponding to $\mathcal{C}^*$, the axial curve of $\mathcal{R}^*$, and recall that throughout $\hat{\mathcal{J}}^*$ the contact force on $\mathcal{R}^*$ has a continuous density $\boldsymbol{f}(\cdot)$.[⋆] In this paper we give examples of equilibrium configurations in which the contact curve is a straight line segment ℓ and the configurations of $\mathcal{R}^*$ and $\mathcal{R}^{**}$ are congruent and related by a 180° rotation about ℓ.[⋆⋆] In such examples the unit vector along the line connecting the centroids of two cross-sections in contact, i.e.,

$$\boldsymbol{v}(s^*) = [\boldsymbol{x}(s^{**}) - \boldsymbol{x}(s^*)]/D, \tag{2.36}$$

is perpendicular to ℓ.

To develop a mathematical theory of solutions of (1.18) appropriate to cases in which the contact curve is straight and (2.36) holds, we let $\boldsymbol{u}$ be the unit vector along ℓ with, for s^* in $\mathcal{J}^*$, $\boldsymbol{u} \cdot \boldsymbol{t}(s^*) > 0$, where $\boldsymbol{t}$ is the unit tangent vector for $\mathcal{C}^*$. We put $\boldsymbol{w}(s^*) = \boldsymbol{u} \times \boldsymbol{v}(s^*)$ and note that the relation (2.36) implies that $\mathcal{C}^*$ is a curve that lies on the surface of a cylinder with axis ℓ and diameter D; moreover, $\mathcal{C}^*$ obeys an equation of the form

$$\boldsymbol{t}(s^*) = \boldsymbol{u} \cos \mu(s^*) - \boldsymbol{w}(s^*) \sin \mu(s^*). \tag{2.37}$$

Such a curve $\mathcal{C}^*$ may be called a *generalized helix* with axis ℓ, winding angle $\mu = \mu(s^*)$, and (constant) radius $D/2$. It follows from (1.14) and (2.37) that throughout

⋆ We keep the assumption made in Section 1 to the effect that a cross-section of $\mathcal{R}$ is not in contact with more than one other cross-section.

⋆⋆ In all cases for which we have found equilibrium configurations of closed knot-free rods, when contact curves have been present they have been segments of straight lines. For rods with the topology of torus knots, we have found circumstances in which an equilibrium configuration occurs with a contact curve that is a circle.

the subsegment $\mathcal{R}^*$ of $\mathcal{R}$

$$\begin{aligned} \boldsymbol{M} &= \left(\frac{2A}{D}\sin^3\mu + C\Delta\Omega\cos\mu\right)\boldsymbol{u} + A\mu'\boldsymbol{v} \\ &\quad + \left(\frac{2A}{D}\sin^2\mu\cos\mu - C\Delta\Omega\sin\mu\right)\boldsymbol{w}. \end{aligned} \tag{2.38}$$

We write $(F_{\mathrm{u}}, F_{\mathrm{v}}, F_{\mathrm{w}})$ for the components of the force $\boldsymbol{F}$ with respect to the basis $(\boldsymbol{u}, \boldsymbol{v}, \boldsymbol{w})$. Employing (2.38), the balance equations (1.18), and the assumption (1.19) that the contact force is normal to the surfaces in contact, we find that $\Delta\Omega$ and F_{u} are constant in s, that

$$F_{\mathrm{v}} = -\left(\frac{6A}{D}\sin\mu\cos\mu - C\Delta\Omega\right)\mu', \tag{2.39}$$

$$F_{\mathrm{w}} = \frac{4A}{D^2}\sin^3\mu + 2\frac{C\Delta\Omega}{D}\cos\mu, \tag{2.40}$$

and that $\mu(\cdot)$ obeys the differential equation,

$$\mu'' - \frac{8}{D^2}\sin^3\mu\cos\mu - \frac{2\omega\Delta\Omega}{D}\cos 2\mu = 0, \tag{2.41}$$

which has the first integral,

$$(\mu')^2 = \frac{4}{D^2}\sin^4\mu + \frac{2\omega\Delta\Omega}{D}\sin 2\mu - q, \tag{2.42}$$

with q a constant. If we write s_0 for the value of s at which the right-hand side of (2.42) would yield $\mu' = 0$, and put $\mu_0 = \mu(s_0)$, then

$$q = \frac{4}{D^2}\sin^4\mu_0 + \frac{2\omega\Delta\Omega}{D}\sin 2\mu_0. \tag{2.43}$$

If we put $\eta = \cot\mu$, (2.42) can be written in the form

$$(\eta')^2 = \hat{P}(\eta); \tag{2.44}$$

here

$$\begin{aligned} \hat{P}(\eta) &= B(\eta - \eta_0)\left[\eta^3 + \frac{\eta_0^2 - \vartheta + 1}{\vartheta\,\eta_0}\eta^2 + \frac{1 + \vartheta + \eta_0^2}{\vartheta}\eta\right. \\ &\qquad \left. + \frac{(\eta_0^2 + 2)\eta_0^2 - \vartheta + 1}{\vartheta\,\eta_0}\right], \end{aligned} \tag{2.45}$$

and

$$\eta_0 = \cot\mu_0, \quad \vartheta = 1 + \omega\Delta\Omega D\eta_0(1 + \eta_0^2), \qquad B = -4\frac{\vartheta}{(1 + \eta_0^2)^2 D^2}. \tag{2.46}$$

The 4 roots of the polynomial $\hat{P}$ are functions of D, ω, $\Delta\Omega$, and μ_0. Once one knows how many of these roots are real numbers, the solution of (2.44), i.e., the integral,

$$s^* - s_0 = \int_{\eta_0}^{\eta} \frac{\mathrm{d}\zeta}{+\sqrt{P(\zeta)}}, \tag{2.47}$$

can be written in terms of elliptic integrals.

For the examples given below in Section 4, $D = 20$, $\omega = 2/3$, $0 < \Delta\Omega < 0.02$, and $-30^\circ < \mu_0 < -10^\circ$, in which range $\hat{P}$ has two real roots, η_0 and η_1, and hence there are numbers b and c for which

$$\hat{P}(\eta) = B(\eta - \eta_0)(\eta - \eta_1)((\eta - b)^2 + c^2), \tag{2.48}$$

and (2.47) reduces to

$$s^* - s_0 = \frac{1}{\sqrt{pq}} \mathrm{F}\left(2 \arctan \sqrt{\frac{q(\eta - \eta_0)}{p(\eta - \eta_1)}} \,\middle|\, m\right), \tag{2.49}$$

where

$$p^2 = ((\eta_0 - b)^2 + c^2), \qquad q^2 = ((\eta_1 - b)^2 + c^2). \tag{2.50}$$

The elliptic integral F in (2.49) is as in (2.14) but has for its modulus

$$m = \frac{1}{2}\sqrt{\frac{(p+q)^2 + (\eta_1 - \eta_0)^2}{pq}}. \tag{2.51}$$

For the winding angle μ of the generalized helix $\mathcal{C}^*$ we obtain the formula,

$$\mu(s^*) = \operatorname{arccot}\left(\frac{q \cot\mu_0 - p \tan^2(\operatorname{sn}((s^* - s_0)\sqrt{pq})/2) \cot\mu_1}{q - p \tan^2(\operatorname{sn}((s^* - s_0)\sqrt{pq}))/2)}\right), \tag{2.52}$$

in which $\cot\mu_1 = \eta_1$ and the elliptic function sn has modulus m.

In view of (2.37), it follows from (2.52) that, once the parameters D and ω are given, the configurations of $\mathcal{R}^*$ and $\mathcal{R}^{**}$ are determined to within a rigid rotation and translation by 4 numbers: the excess twist density $\Delta\Omega$, the arc-length parameters s_a^*, s_b^* of the end points of $\mathcal{R}^*$, and the winding angle μ_0 at the point s_0 on the solution of (2.41) where the right-hand side of (2.42) vanishes. Although we here give examples of configurations for which s_0 corresponds to a cross-section in $\mathcal{R}^*$,[⋆] such need not always be the case.

As in the theory of isolated points of self-contact, the procedure for determining $\mathcal{C}^*$ from $\Delta\Omega$, μ_0, s_a^*, and s_b^*, yields also the components, with respect to the Serret–Frenet triad $(\boldsymbol{t}, \boldsymbol{n}, \boldsymbol{b})_a^*$ at s_a^*, of the vector

$$\boldsymbol{h}^* = \boldsymbol{x}(s_b^*) - \boldsymbol{x}(s_a^*), \tag{2.53}$$

[⋆] For the supercoiled configurations depicted in Figure 7, which, incidentally, are global minimizers of Ψ at fixed $\Delta\mathcal{L}$, s_0 is the arc-length parameter of the midpoint of $\mathcal{C}^*$.

the orthogonal tensor $\boldsymbol{Q}^*$ that takes $(\boldsymbol{t}, \boldsymbol{n}, \boldsymbol{b})^*_a$ into $(\boldsymbol{t}, \boldsymbol{n}, \boldsymbol{b})^*_b$, and, by (2.39) and (2.40), the vectors $\boldsymbol{F}^*_{a^+} = \lim_{s \to s^*_{a^+}} \boldsymbol{F}(s)$ and $\boldsymbol{F}^*_{b^-} = \lim_{s \to s^*_{b^-}} \boldsymbol{F}(s)$.

In the general case in which an equilibrium configuration $(\mathcal{C}, \Delta\Omega)$ of $\mathcal{R}$ has N pairs of cross-sections that are in contact at isolated contact points, and, in addition, J pairs $(\mathcal{R}^*, \mathcal{R}^{**})_j$ of subsegments that are in contact along contact curves, $\mathcal{R}$ can be decomposed* into $2N + 4J + 1$ subsegments $\mathcal{R}_i$ of two types: (I) subsegments that are contact-free everywhere except for their ends (and hence correspond to single edges in Figure 1), and (II) subsegments that are in continuous contact along their length (and hence correspond to double edges). At each s_i characterizing a cross-section that separates any two of these $2N+4J+1$ subsegments that abut, the contact force is a concentrated force (regardless of the type of the subsegments). The configuration of a subsegment $\mathcal{R}_i$ of type I is given by the formulae (2.8)–(2.10) and is determined by a sextuple of parameters $(a_i, \lambda_i, T_i, \sigma_i^-, \sigma_i^+, L_i)$, while subsegments of type II form conjugate pairs $(\mathcal{R}^*, \mathcal{R}^{**})_j$, where the configuration of each pair is given by (2.37) and (2.42)** and is determined by a quadruple of parameters $(\Delta\Omega_j, (\mu_0)_j, (s^*_a)_j, (s^*_b)_j)$.

Once a value has been assigned to the excess link of $\Delta\mathcal{L}$ of $\mathcal{R}$ and a particular contact diagram has been assumed, one knows, for each $i = 1, \ldots, 2N + 4J + 1$, the type of the subsegment $\mathcal{R}_i$ and the index k of the cross-section (at s_k) that is in contact with the cross-section at the endpoint of $\mathcal{R}_i$ at s_i. The problem of determining the $12N + 16J + 6$ solution parameters that make up the parameter set

$$\begin{aligned} \mathcal{Q} \;=\; & \{a_i, \lambda_i, T_i, \sigma_i^-, \sigma_i^+, L_i \mid i = 1, 2, \ldots, 2N + 2J + 1\} \\ & \cup \{\Delta\Omega_j, (\mu_0)_j, (s^*_a)_j, (s^*_b)_j \mid j = 1, 2, \ldots, J\} \end{aligned} \tag{2.54}$$

then reduces to one of solving a system $\mathcal{E}$ of $12N + 16J + 6$ algebraic equations. In this general case the algebraic equations making up $\mathcal{E}$ result from: (i) the equation $\Delta\mathcal{T} + \mathcal{W} = \Delta\mathcal{L}$, (ii) the closure conditions (1.20), (iii) the relation (2.30), and (iv) the requirements that (1.15)–(1.17) and (1.19) hold for each s_i and that, in the interior of the interval of s corresponding to a subsegment $\mathcal{R}_i$, (1.13) holds if $\mathcal{R}_i$ is of type I and (1.15), (1.16), (1.18), and (1.19) hold if $\mathcal{R}_i$ is of type II.

3. Stability

A pair $(\mathcal{C}^\#, \Delta\Omega^\#)$ that obeys the constraints imposed on $\mathcal{R}$, which include its impenetrability and the closure conditions, is here called a *configuration*. One may be tempted to say that this configuration is in equilibrium if it obeys equations (1.13)–(1.20). However, in general theories, such as the present in which a body is assumed to be impenetrable, the definition of a state of equilibrium is a matter that requires care.

* See footnote ** on page 182.

** I.e., (2.47), or, in the present case, (2.52).

Let $\mathfrak{S}$ be the set of smooth homotopies $\mathcal{H} : \eta \mapsto (\mathcal{C}_\eta, \Delta\Omega_\eta)$ with $(\mathcal{C}_\eta, \Delta\Omega_\eta)|_{\eta=0} = (\mathcal{C}^\#, \Delta\Omega^\#)$ that are *admissible* in the sense that for each η the pair $(\mathcal{C}_\eta, \Delta\Omega_\eta)$ is a configuration and $\Delta\mathcal{L}$ is independent of η.[⋆] We say that $(\mathcal{C}^\#, \Delta\Omega^\#)$ is an *equilibrium configuration* if, for each $\mathcal{H}$ in $\mathfrak{S}$:

(a) the equation

$$\frac{\mathrm{d}}{\mathrm{d}\eta}\Psi(\mathcal{C}_\eta, \Delta\Omega_\eta)\Big|_{\eta=0} = 0 \tag{3.1a}$$

holds when the domain of $\mathcal{H}$ is an interval of the form $-\varepsilon < \eta < \varepsilon$, and

(b) the relation (with one-sided derivative)

$$\frac{\mathrm{d}}{\mathrm{d}\eta}\Psi(\mathcal{C}_\eta, \Delta\Omega_\eta)\Big|_{\eta=0+} \geqslant 0 \tag{3.1b}$$

holds when the domain of $\mathcal{H}$ has the form $0 \leqslant \eta < \varepsilon$.

It is clear that, for a configuration $(\mathcal{C}^\#, \Delta\Omega^\#)$ that obeys (b), equality must hold in (3.1b) whenever the homotopy $\mathcal{H}$ in $\mathfrak{S}$ with domain $0 \leqslant \eta < \varepsilon$ can be smoothly extended to a homotopy in $\mathfrak{S}$ with domain $-\varepsilon < \eta < \varepsilon$. Hence (b) implies (a). However, the converse is not true, (a) does not imply (b). If $\mathcal{R}$ has points of self-contact when in the configuration $(\mathcal{C}^\#, \Delta\Omega^\#)$, the set $\mathfrak{S}$ contains homotopies that are "intrinsically one-sided" in that they cannot be extended from $0 \leqslant \eta < \varepsilon$ to $-\varepsilon < \eta < \varepsilon$.

If a configuration $(\mathcal{C}^\#, \Delta\Omega^\#)$ showing points of self-contact obeys (a) then for it all of the equations (1.13)–(1.20) hold.[⋆⋆] If, in addition, it obeys (b), then it is such that the contact force exerted on a cross-section by another is directed toward the interior of the first, i.e., pushes the first away, rather than pulls it in. In other words, in the present theory a configuration obeying (b) not only obeys the governing equations (1.13)–(1.20) but also the following condition:

Condition C: When two cross-sections, at s^* and s^{**} with $s^* \neq s^{**}$, are in contact, $f(s^*)$ in (1.19) is not negative.

Arguments of the type just given can be employed to construct a formal proof of the following remark: *An equilibrium configuration is a solution of* (1.13)–(1.20) *that obeys the conditions* Γ *and* C. As $\Delta\Omega$ is independent of s at equilibrium, an equilibrium configuration is specified when the pair $(\mathcal{C}, \Delta\mathcal{T})$ is given.

Here, as in [1] and [2], a configuration $(\mathcal{C}^\#, \Delta\Omega^\#)$ is said to be *stable* if it gives a strict local minimum to Ψ in the class of configurations compatible with the

[⋆] As $\mathcal{H}$ is a smooth homotopy compatible with the impenetrability of $\mathcal{R}$, it preserves the knot-type of $\mathcal{C}$.

[⋆⋆] This conclusion rests on the assumption, made throughout the paper, that Ψ obeys the equations (1.4)–(1.6) and that the following equations hold: (1.15) and (1.16), which are consequences of the impenetrability of $\mathcal{R}$; (1.19) stating that the contact forces are shear-free; and (1.20) expressing the fact that $\mathcal{R}$ is a closed rod. These equations are employed in the derivation of (1.13), (1.14), (1.17), (1.18) from the assumption that (a) holds.

constraints. In other words, $(\mathcal{C}^{\#}, \Delta\Omega^{\#})$ is stable if, and only if, it has a neighborhood* $\mathcal{N}$ such that $\Psi(\mathcal{C}, \Delta\Omega) > \Psi(\mathcal{C}^{\#}, \Delta\Omega^{\#})$ for each configuration $(\mathcal{C}, \Delta\Omega)$ in $\mathcal{N}$ that is not equivalent** to $(\mathcal{C}^{\#}, \Delta\Omega^{\#})$ and, in addition, is accessible from $(\mathcal{C}^{\#}, \Delta\Omega^{\#})$ by an admissible homotopy.

We call a configuration $(\mathcal{C}^{\#}, \Delta\Omega^{\#})$ *differentially stable*, if, for each $\mathcal{H}$ in $\mathfrak{S}$ with domain $0 \leqslant \eta < \varepsilon$, either

$$\frac{\mathrm{d}}{\mathrm{d}\eta}\Psi(\mathcal{C}_\eta, \Delta\Omega_\eta)\Big|_{\eta=0+} > 0 \tag{3.2a}$$

or

$$\frac{\mathrm{d}}{\mathrm{d}\eta}\Psi(\mathcal{C}_\eta, \Delta\Omega_\eta)\Big|_{\eta=0+} = 0 \quad \text{and} \quad \frac{\mathrm{d}^2}{\mathrm{d}\eta^2}\Psi(\mathcal{C}_\eta, \Delta\Omega_\eta)\Big|_{\eta=0+} \geqslant 0. \tag{3.2b}$$

Of course, a differentially stable configuration obeys (b) and hence is an equilibrium configuration.

If a configuration $(\mathcal{C}^{\#}, \Delta\Omega^{\#})$ is a member of a one-parameter family E of equilibrium configurations for which one can take $\Delta\mathcal{L}$, Ψ, and $\mathcal{C}$ to be given by functions of $\mathcal{W}$, then in order for $(\mathcal{C}^{\#}, \Delta\Omega^{\#})$ to be stable it is necessary that, for the family E, the slope of the graph of $\Delta\mathcal{L}$ versus $\mathcal{W}$, i.e., $\mathrm{d}\Delta\mathcal{L}^E/\mathrm{d}\mathcal{W}$, be not negative at $(\mathcal{C}^{\#}, \Delta\Omega^{\#})$. A proof that this relation

$$\mathrm{d}\Delta\mathcal{L}^E/\mathrm{d}\mathcal{W} \geqslant 0, \tag{3.3}$$

which we call *condition* E,‡ is a necessary condition for stability, was given in [1].‡‡

It is worth mentioning that there are exceptional families of equilibrium configurations for which $\Delta\mathcal{L}$ is *not* determined by $\mathcal{W}$, because, for them, equilibrium is maintained when $\Delta\mathcal{L}$ is changed with $\mathcal{C}$ kept constant. Such is the case for configurations in which $\mathcal{C}$ is a true circle, i.e., the configurations that form the "trivial branch" of a bifurcation diagram.

Condition E is necessary but far from sufficient for even differential stability. In [1] and [2] it was pointed out that following stronger condition, called *condition* θ, is necessary for differential stability and yields a practical method of demonstrating that certain configurations that obey condition E are in fact unstable: An equilibrium configuration $(\mathcal{C}^{\#}, \Delta\mathcal{T}^{\#})$ is said to obey condition θ if for each ξ with $0 < \xi \leqslant L$ there holds $\theta(\xi) \geqslant 0$, where $\theta(\xi)$ is the minimum value of $\mathrm{d}\Delta\mathcal{L}/\mathrm{d}\mathcal{W}$ at $(\mathcal{C}^{\#}, \Delta\mathcal{T}^{\#})$ for the families¶ of equilibrium configurations of the plasmid that are

* For the present purpose it is not essential to completely specify the topology on the set of configurations.

** $(\mathcal{C}^{\#}, \Delta\Omega^{\#})$ and $(\mathcal{C}, \Delta\Omega)$ are equivalent if $\Delta\Omega^{\#} = \Delta\Omega$ and $\mathcal{C}^{\#}$ is congruent to $\mathcal{C}$.

‡ A condition that, in the present context, is equivalent to condition E may be found in a seminal paper of Le Bret [14].

‡‡ The theory of [1] is more general than the present in that it is applicable to cases in which external forces act on a rod which may be closed or open and subject to appropriate end conditions.

¶ In all practical cases there is only one such family.

subject to the additional (artificial) condition that the subsegment with $\xi \leqslant s < L$ be held rigid.*

In recent and as yet unpublished work, we prove that (i) for equilibrium configurations without self-contact, condition θ is sufficient for differential stability, and (ii) whether or not self-contact is present, for an equilibrium configuration to be stable it is necessary, not only that $\theta(\xi) \geqslant 0$ for $0 < \xi \leqslant L$, but also that

$$\theta(\xi) \geqslant \min\{1, \theta(L)\} \quad \text{for} \quad 0 < \xi \leqslant L. \tag{3.4}$$

In order for a configuration $(\mathcal{C}^{\#}, \Delta\Omega^{\#})$ to be differentially stable it is necessary that the axial curve $\mathcal{C}$ give a local minimum to the bending energy Ψ_{B} at fixed writhe, i.e., in the class of curves that obey the imposed constraints and have the same writhe as $\mathcal{C}$. In particular, differential stability of $(\mathcal{C}^{\#}, \Delta\Omega^{\#})$ requires that *condition* W hold,** i.e., that for each $\mathcal{H}$ in $\mathfrak{S}$ with domain $0 \leqslant \eta < \varepsilon$ and with $\mathcal{W}(\mathcal{C}_\eta)$ independent of η either

$$\frac{\mathrm{d}}{\mathrm{d}\eta}\Psi_{\mathrm{B}}(\mathcal{C}_\eta)\Big|_{\eta=0+} > 0 \tag{3.5a}$$

or

$$\frac{\mathrm{d}}{\mathrm{d}\eta}\Psi_{\mathrm{B}}(\mathcal{C}_\eta)\Big|_{\eta=0+} = 0 \quad \text{and} \quad \frac{\mathrm{d}^2}{\mathrm{d}\eta^2}\Psi_{\mathrm{B}}(\mathcal{C}_\eta)\Big|_{\eta=0+} \geqslant 0. \tag{3.5b}$$

Arguments given in [1] show that strengthened versions of conditions E and W can be combined to obtain a condition, called *condition* S, that is *sufficient* for stability.‡ An equilibrium configuration $(\mathcal{C}^{\#}, \Delta\Omega^{\#})$ in the family E obeys condition S if $\mathrm{d}\Delta\mathcal{L}^E/\mathrm{d}\mathcal{W} > 0$ at $(\mathcal{C}^{\#}, \Delta\Omega^{\#})$, and, in addition, $(\mathcal{C}^{\#}, \Delta\Omega^{\#})$ has a neighborhood $\mathcal{N}$ such that, for each configuration $(\mathcal{C}^E, \Delta\Omega^E)$ in $\mathcal{N}$ and E, there holds $\Psi_{\mathrm{B}}(\mathcal{C}) > \Psi_{\mathrm{B}}(\mathcal{C}^E)$ for every accessible configuration‡‡ in $\mathcal{N}$ for which $\mathcal{C}$ has the same writhe as, but is not congruent to, $\mathcal{C}^E$.

Although it is often possible to use condition W to prove that an equilibrium configuration is *not* stable,¶ with the exception of those configurations that lie on a special primary branch of the bifurcation diagram (called branch α), it is, in general, difficult to use condition S to prove that a configuration *is* stable.

4. Calculated Configurations and Bifurcation Diagrams

We here present configurations and bifurcation diagrams for equilibrium configurations of closed rods calculated using the method explained in Section 2. The results given are for rods with $d = 8.2 \times 10^{-3}$. For DNA, if one takes D to be equal to

* Condition E is equivalent to the assertion that $\theta(\xi)$ be non-negative when $\xi = L$.
** Cf. [1] and [2].
‡ [1], page 751.
‡‡ A configuration is accessible from $(\mathcal{C}^{\#}, \Delta\Omega^{\#})$ if and only if it is accessible from $(\mathcal{C}^E, \Delta\Omega^E)$.
¶ Cf. [2], page 765.

its steric value, 20 Å, the employed value of d becomes appropriate to a plasmid that contains 718 base pairs.[⋆] For the ratio $\omega = C/A$ we use the value $2/3$ which holds for rods of circular cross-section formed from elastic materials that are both isotropic and incompressible, and hence have Poisson's ratio ν equal to 1/2.[⋆⋆] DNA is not an isotropic material, and there is experimental evidence to the effect that values of ω larger than $2/3$ are appropriate for it.[‡] However, at the end of the paper, after we point out that results given in [1] tell us that, once the bifurcation diagram and equilibrium configurations are known (in a range of $\Delta\mathcal{L}$) for one closed rod, they can be found by scaling arguments for other closed rods that have the same d but different values of ω (and values of $\Delta\mathcal{L}$ that lie in appropriate ranges that depend on ω),[‡‡] we use our results for $\omega = 2/3$ to obtain (for illustrative purposes) a bifurcation diagram for $\omega = 8/5$.

A closed rod $\mathcal{R}$ with ω, d, and $\Delta\mathcal{L}$ specified has at least one and usually several equilibrium configurations (see, e.g., Figures 2 and 3). When $\Delta\mathcal{L}$ is varied with ω and d held fixed, one-parameter families of equilibrium configurations are obtained. We here focus on, but do not confine attention to, continuous sets of such families, called *branches*, that are connected to a family (called the *trivial branch*) that is made up of the configurations for which $\mathcal{C}$ is a circle and hence $\mathcal{W} = 0$.[¶] In the bifurcation diagrams that we present, the trivial branch is labeled ζ and is shown as a dotted line; *primary branches*, i.e., α, β, ... originate at bifurcation points of the trivial branch and are shown as solid curves. Branches that originate at bifurcation points of a primary branch (and hence are connected to ζ by one branch) are called *secondary branches*; they are given labels that bear subscripts, i.e., β_{I}, β_{II}, ..., γ_{I}, γ_{II}, ..., and are drawn with dashed curves (in Figures 13, 15, 17, and 29 below). *Tertiary branch* also occurs; an example is the branch β^*_{II} which

[⋆] To account in an approximate way for the electrostatic self-repulsion of DNA one may take D to be larger than its steric value D_σ. If one does so, the number of base pairs (or value of L) corresponding to a given d is to be increased in proportion to the ratio D/D_σ.

[⋆⋆] For rods of circular cross-section formed from isotropic elastic materials $C/A = (1+\nu)^{-1}$ (cf., e.g., [19]).

[‡] If we set A equal to 2×10^{-11} erg Å (which corresponds to a persistence length $A/k_{\mathrm{B}}T$ of 500 Å at $T = 298$ K; cf. [23]), the choice $\omega = 2/3$ becomes compatible with measurements of fluorescence polarization anisotropy of dyes intercalated in open segments of DNA (see [24]), but measurements of topoisomer distributions for miniplasmids [25] then imply that ω should be close to 1.4. (See also Bouchiat and Mezard [26] who state that single molecule stretching experiments [27] (with force and specific linking number controlled) yield a value of 1.6, i.e., 8/5, for ω.) That the value of ω for DNA seems to depend on the method of measurement is a matter of current interest and concern in biophysics (cf. [28]) and indicates that one should be cautious in the application to DNA of quantitative results based on the special case of Kirchhoff's constitutive relations that is appropriate for rods that are homogenous, inextensible, and axially symmetric.

[‡‡] Cf. [1], equations (39) and (40).

[¶] In the present theory there are families of equilibrium configurations that are not connected to the trivial branch by continuous families of solutions of (1.13)–(1.20) that are physically acceptable in that they obey condition Γ. Examples are the families labeled $\bar{\beta}_{\mathrm{I}}$, $\bar{\beta}_{\mathrm{II}}$, $\bar{\beta}^*_{\mathrm{II}}$, $\bar{\beta}_{\mathrm{III}}$, $\bar{\beta}_{\mathrm{IV}}$ in Figures 20 and 22.

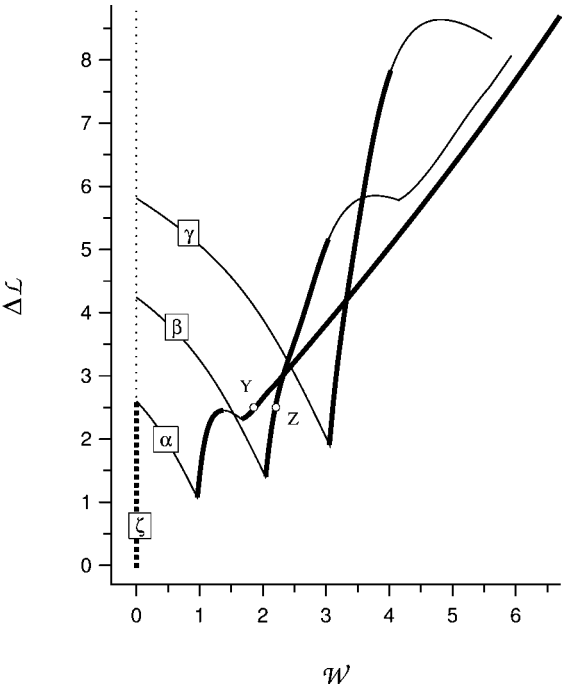

Figure 3. Bifurcation diagram drawn as a plot of $\Delta\mathcal{L}$ versus $\mathcal{W}$ and showing the bifurcations of the trivial branch ζ (dotted vertical line) that give rise to primary branches, α, β, γ (solid curves). Here (as in Figure 2 and also in Figures 4–30) $\omega = 2/3$; throughout the paper $d = 8.2 \times 10^{-3}$. The points at which primary branches overlap are not points of bifurcation. The points labeled Y and Z correspond to the configurations shown in Figure 2. Here (and in Figures 4–6, 11, 13, 15, 17, 20, 22, 29, 31–33) the regions of branches comprised of unstable equilibrium configurations are drawn as light solid, dotted, or dashed curves. In the case of branch ζ, large dots indicate a region in which configurations are stable.

originates at a point of the secondary branch β_{II}. (The branch β^*_{II} appears in Figure 13 as a curve drawn with short dashes.)

As the elastic rings we are considering are such that to each equilibrium configuration there corresponds a complementary equilibrium configuration with $\Delta\mathcal{L}$ replaced by $-\Delta\mathcal{L}$ and $\mathcal{C}$ by its mirror image, and hence with $\mathcal{W}$ replaced by $-\mathcal{W}$ and $\Delta\mathcal{T}$ by $-\Delta\mathcal{T}$, we take $\Delta\mathcal{L}$ to be positive.

Each point on the branch ζ for which

$$\Delta\mathcal{L} = \omega^{-1}\sqrt{m^2 - 1}, \quad m = 2, 3, 4, \ldots, \tag{4.1}$$

is a bifurcation point at which a primary branch originates.⋆ We call m the *index* of the corresponding primary branch and label those branches so that $m = 2$ for α, $m = 3$ for β, etc. The symmetry group of the configurations forming the primary branch with index m is D_m, the dihedral group of order $2m$. Thus, whether or not

⋆ The linear analysis giving (4.1) is familiar in rod theory (see, e.g., [29] for the case $m = 2$).

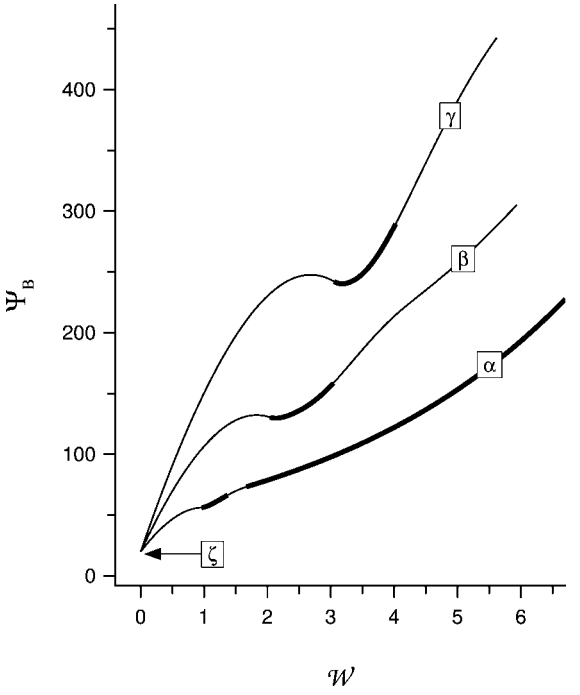

Figure 4. Graphs of Ψ_B versus $\mathcal{W}$ for the primary branches α, β, γ. Here the trivial branch ζ reduces to a single point with $\mathcal{W} = 0$. As in Figures 5, 24–28, 32, 33, the energies Ψ_B and Ψ are dimensionless, i.e., are given in units of A/L (cf. [1, 7]).

self-contact is present, the curve $\mathcal{C}$ for a configuration on the primary branch with index m has an axis $\mathcal{A}_m$ of m-fold symmetry that is perpendicular to the plane $\mathcal{P}$ containing the $2m$ points at which κ has a local maximum or a local minimum; each of the m straight lines that intersect $\mathcal{A}_m$ and pass through two extrema of κ is an axis of 2-fold symmetry.*

Graphs of $\Delta\mathcal{L}$ versus $\mathcal{W}$ for the primary branches α, β, and γ are given in Figure 3. See Figures 4 and 5 for the corresponding graphs of Ψ_B versus $\mathcal{W}$ and Ψ versus $\Delta\mathcal{L}$.

PRIMARY BRANCH α

Details of the graph of $\Delta\mathcal{L}$ versus $\mathcal{W}$ for the branch α can be seen in Figure 6. For $n = 0$, 1, 2, and 3, the configurations with n points of self-contact correspond to points on that graph between A^n and A^{n+1}. The configuration A^0 (at which α

* For closed rods obeying the present assumptions, Domokos [30] proved that each contact-free equilibrium configuration has D_n symmetry, which is what was found in the present study. In the same paper he conjectured that the symmetry group of an equilibrium configuration with self-contact contains C_2 as a subgroup, which is not the case for configurations in the tertiary branch β^*_{II}. A very recent paper of Domokos and Healey [31] contains an important extension of the results given in [30].

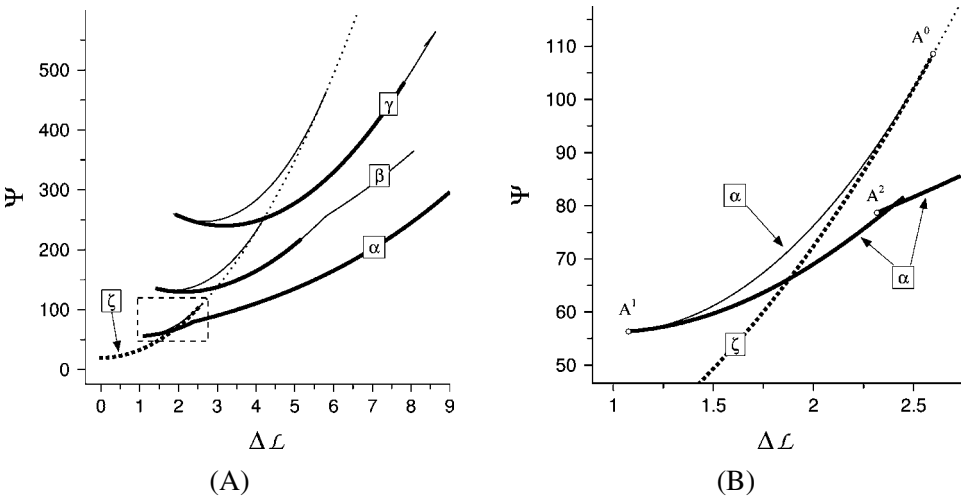

Figure 5. (A) Graphs of Ψ versus $\Delta\mathcal{L}$ for branches ζ, α, β, γ. (B) An enlargement of the rectangular region bounded by dashed lines in (A).

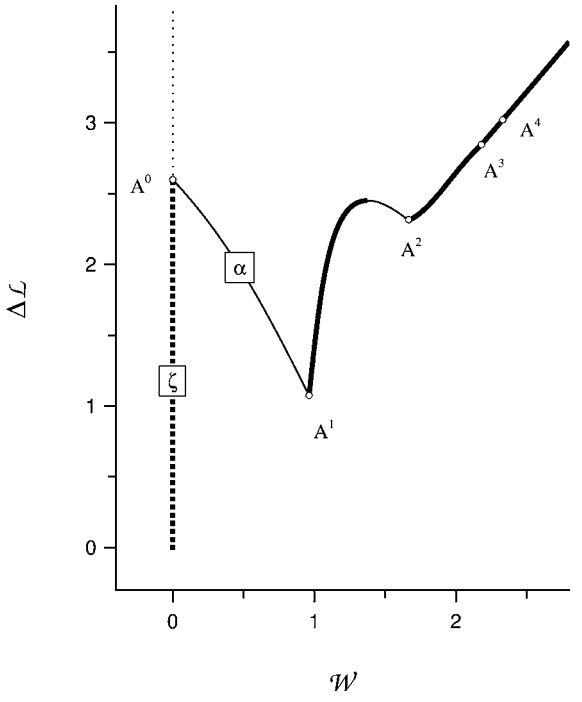

Figure 6. Graphs of $\Delta\mathcal{L}$ versus $\mathcal{W}$ for branch α. Configurations corresponding to the labeled points are shown in Figure 7.

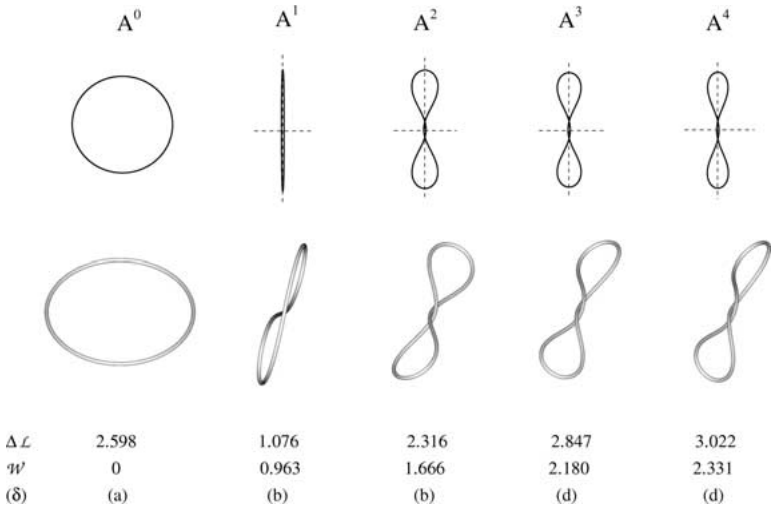

Figure 7. For each n, A^n is the configuration in α with a writhe $\mathcal{W}(A^n)$ equal to the infimum of the writhe of configurations in α with n or more points of self-contact. The top row shows the projection of $\mathcal{C}$ on the plane $\mathcal{P}$; 2-fold symmetry axes in $\mathcal{P}$ are shown as dashed lines. The line of view for the bottom row is at 75° from $\mathcal{P}$. The scale is reduced in the top row relative to the second row, but is constant within each row.

branches off from ζ), the configuration A^1 (which resembles a "figure 8") and the configurations A^2, A^3, A^4 are shown in Figure 7. Each configuration in α (including those showing self-contact, whether at points or along intervals) has D_2 symmetry, i.e., has three axes of 2-fold symmetry, two of which lie in the plane $\mathcal{P}$ and are such that one contains the two points of maximum curvature for $\mathcal{C}$ and the other the points of minimum curvature. The dependence on $\mathcal{W}$ of the arc-length locations of cross-sections that are in contact is given in Figure 8, where the point at which $s = 0$ is chosen to be a point of maximum curvature. That figure, although it depends on the choice of d, is independent of ω and shows that for $\mathcal{W}$ between $\mathcal{W}(A^1)$ and $\mathcal{W}(A^2)$ self-contact occurs at the two values of s where $\kappa(s)$, the curvature of $\mathcal{C}$, attains its minimum (i.e., where s/L is equal to 1/4 or 3/4). At $\mathcal{W} = \mathcal{W}(A^2)$ the point of self-contact divides into two points with an arc-length separation that increases with $\mathcal{W}$. At $\mathcal{W} = \mathcal{W}(A^3)$ a new self-contact occurs where κ has a minimum, and for $\mathcal{W}(A^3) \leqslant \mathcal{W} \leqslant \mathcal{W}(A^4)$ the rod contains three points of self-contact: one where κ has a minimum and two with an arc-length separation that increases with $\mathcal{W}$. Configurations with $\mathcal{W} > \mathcal{W}(A^4)$ have two isolated points of self-contact and a contact curve for which the corresponding intervals* of s are centered at $s/L = 1/4$ and 3/4.

In summary: For a configuration in α with writhe $\mathcal{W} \geqslant 0$ there are no points of self-contact for $\mathcal{W} < \mathcal{W}(A^1)$, there is one such point for $\mathcal{W}(A^1) \leqslant \mathcal{W} \leqslant \mathcal{W}(A^2)$, two for $\mathcal{W}(A^2) < \mathcal{W} < \mathcal{W}(A^3)$, three for $\mathcal{W}(A^3) \leqslant \mathcal{W} \leqslant \mathcal{W}(A^4)$, and an interval

* The reader will recall that a contact curve corresponds to 2 distinct intervals of s.

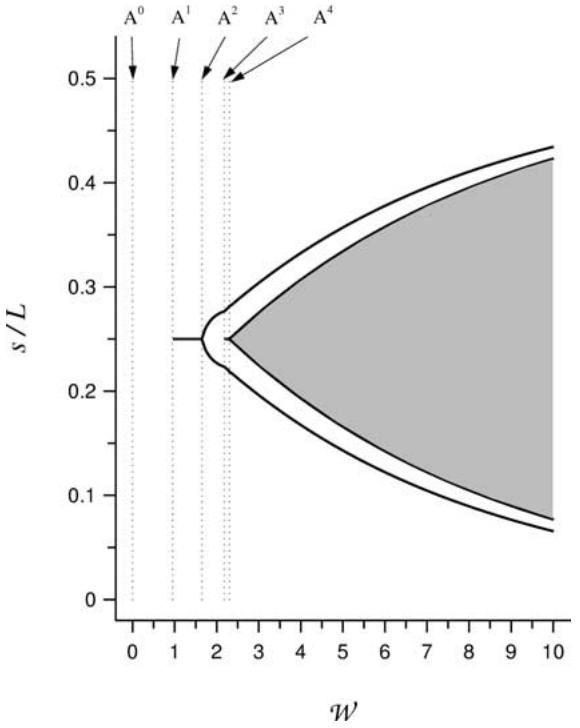

Figure 8. Dependence on $\mathcal{W}$ of the arc-length locations of cross-sections that are in contact when the configuration is in the branch α. Because these configurations have D_2 symmetry, results are shown only for $0 < s/L < 1/2$. The shaded area gives for each $\mathcal{W}$ the range of s/L that corresponds to the line of contact; the solid curves give s/L for isolated points of self-contact and endpoints of the line of contact.

of self-contact as well as two isolated points of self-contact for $\mathcal{W} > \mathcal{W}(\mathrm{A}^4)$. Hence there is no configuration in α with precisely 4 points of self-contact.⋆

We wish to emphasize that, as Figure 8 illustrates, in Kirchhoff's theory of inextensible rods of circular cross-section with d not too large, for a closed rod with sufficiently high excess link, a configuration in branch α shows both a contact curve⋆⋆ and two isolated points of self-contact, and the length of *each* contact-free subsegment of $\mathcal{R}$ decreases with increasing $\Delta\mathcal{L}$.

Configurations in α with intervals of self-contact are shown in Figure 9. In the present case, the equations (2.36)–(2.52) tell us that the winding angle μ of the generalized helix giving $\boldsymbol{x}(s^*)$ for s^* in $\mathcal{J}^*$ is negative and nearly, but not exactly, constant over $\mathcal{J}^*$.‡ The minimum value of $|\mu|$ in $\mathcal{J}^*$, μ_0, is attained at the center

⋆ This description of the writhe-dependence of self-contact for configurations in α, although independent of ω, does depend on $d = D/L$ and cannot hold for d above a critical value.

⋆⋆ Here that curve is a straight line and hence can be called a *line of contact*.

‡ The present theory of self-contact in closed rods has the following properties not shared by recent approximate theories that rest on the assumption that $\mathcal{C}^*$ is a true helix (cf., e.g., [32]): (i)

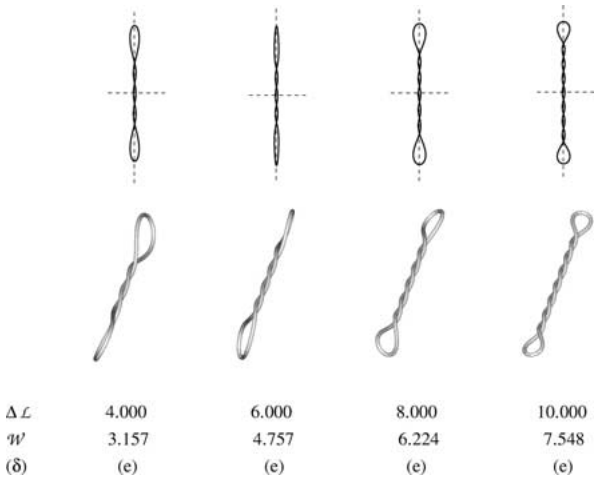

Figure 9. Selected configurations in branch α with intervals of self-contact.

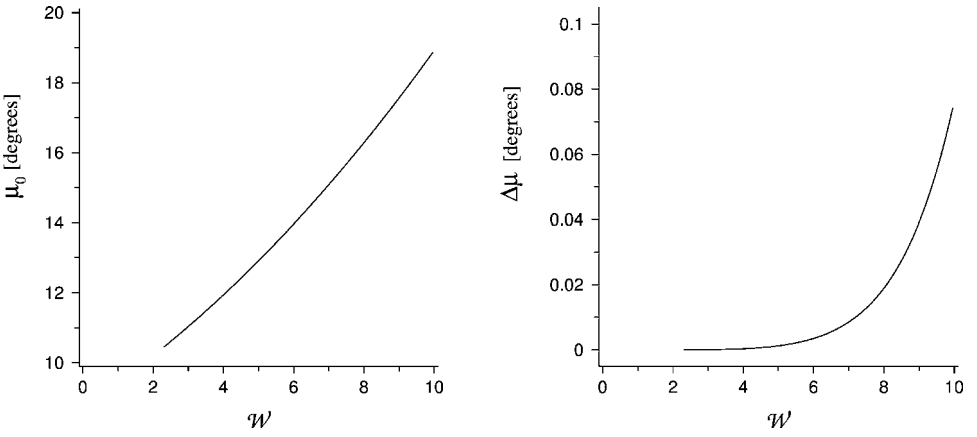

Figure 10. Dependence on $\mathcal{W}$ of: μ_0, the winding angle of $\mathcal{C}$ at the center of (straight) contact curves for configurations in α, and $\Delta\mu$, the width of the range of attained winding angles.

and of $\mathcal{J}^*$ and the maximum value, $\bar{\mu}$, of $|\mu|$ at the end points of $\mathcal{J}^*$. As seen in Figure 10, both μ_0 and the difference, $\Delta\mu = \bar{\mu} - \mu_0$, increase with increasing $\mathcal{W}$.

As each configuration in α gives a strict global minimum to Ψ_B in the class of *all* configurations with the same value of $\mathcal{W}$ (see, e.g., Figure 4), we can apply the

equation (2.52) here gives an exact expression for the departure of μ from a constant value; (ii) here one can show that the terminal loops associated with intervals of self-contact contain isolated points of self-contact. The observations (i) and (ii), as they apply to all configurations of a knot-free closed rod with intervals of self-contact, are not restricted to configurations in branch α.

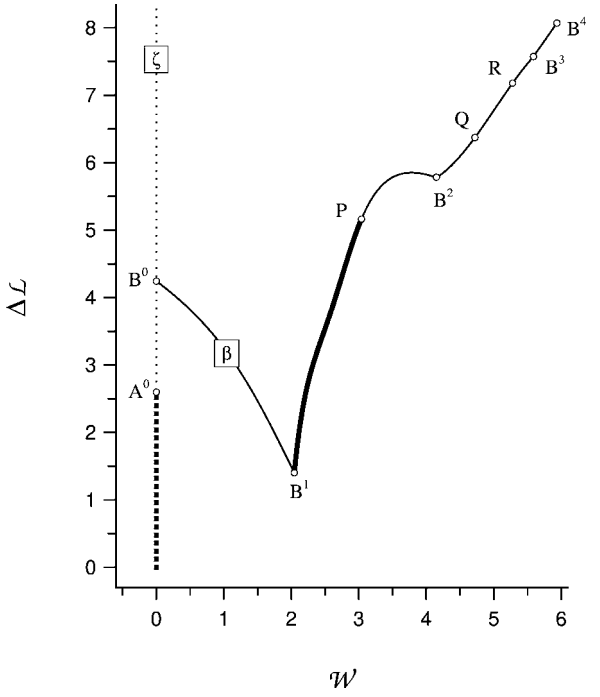

Figure 11. Graphs of $\Delta\mathcal{L}$ versus $\mathcal{W}$ for branch β . Configurations corresponding to the labeled points are shown in Figures 12 and 18.

condition S and assert that a configuration in α is stable whenever

$$\left(\frac{\mathrm{d}\Delta\mathcal{L}}{\mathrm{d}\mathcal{W}}\right)_+ > 0, \qquad \left(\frac{\mathrm{d}\Delta\mathcal{L}}{\mathrm{d}\mathcal{W}}\right)_- > 0, \tag{4.2}$$

where the one-sided derivatives are computed along the branch α.*

As $(\mathrm{d}\Delta\mathcal{L}/\mathrm{d}\mathcal{W})_+$ and $(\mathrm{d}\Delta\mathcal{L}/\mathrm{d}\mathcal{W})_-$ are both positive at A^3 and A^4, those configurations are stable. At A^1 and A^2, $(\mathrm{d}\Delta\mathcal{L}/\mathrm{d}\mathcal{W})_+ > 0$, $(\mathrm{d}\Delta\mathcal{L}/\mathrm{d}\mathcal{W})_- < 0$, and the graph of $\Delta\mathcal{L}$ versus $\mathcal{W}$ has a local maximum between A^1 and A^2. We say that A^1, A^2, and the local maximum between them are *points of exchange of stability*.

For each $\Delta\mathcal{L}$ exceeding a critical value $(\Delta\mathcal{L})^\dagger$ that depends on d and ω, there is a configuration in α that gives not only a local but also a global minimum to the elastic energy Ψ, a conclusion that is in accord with the calculation shown in Figure 5. In the present case, $(\Delta\mathcal{L})^\dagger = 1.880$.

* The left- and right-handed derivatives of this type are equal for all configurations in a branch with the exception of those at which there is a change in the number of points of self-contact.

For a thorough treatment of a similar case, i.e., that in which ω is 1.5 and d has twice the present value, see [2], which contains graphs of Ψ_{B} versus $\mathcal{W}$ and Ψ versus $\Delta\mathcal{L}$ that show several secondary branches.

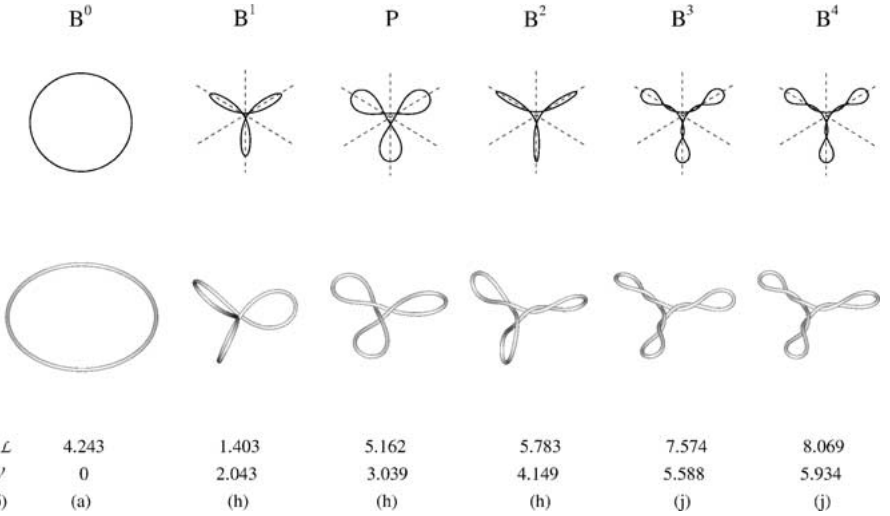

Figure 12. Selected configurations in branch β. As explained in the text, the configurations in β between B^n and B^{n+1} have $3n$ points of self-contact; P and B^1 are configurations at points of secondary bifurcation for β.

PRIMARY BRANCH β AND ITS HIGHER-ORDER DESCENDANTS

The graph of $\Delta\mathcal{L}$ versus $\mathcal{W}$ for the primary branch β, which originates at B^0, i.e., at the point on ζ where $\Delta\mathcal{L} = 2\sqrt{2}/\omega$, is shown in Figure 11. The configurations in β have D_3 symmetry. For $n = 0$, 1, 2, and 3, the points lying between B^n and B^{n+1} in Figure 11 correspond to configurations with $3n$ points of self-contact. Each configuration in β with $\mathcal{W} \geqslant \mathcal{W}(B^1)$, including B^1, P, B^2, B^3, and B^4 which are shown in Figure 12, contains three congruent loops. In this paper, as in [2], when we call a subsegment of a closed rod a loop, we presuppose that its ends are in contact. At sufficiently large values of $\mathcal{W}$, a loop shows self-contact not only at its end points, but also in its interior. (Such is the case here when $\mathcal{W} > \mathcal{W}(B^2)$.) It is in agreement with current usage to call a loop of DNA with more than one self-contact a *plectonemic loop*, or a *plectoneme*.

The points B^1, P, Q, and R in Figure 11 are bifurcation points at which β meets with the secondary branches β_{I}, β_{II}, β_{III}, β_{IV}, and β_{V} (see Figures 13–18). These secondary branches are comprised of configurations that have C_2 symmetry (characterized by the presence of a single axis of 2-fold symmetry) and hence have a symmetry group that is a proper subgroup of D_3.*

* The following convention, familiar in bifurcation theory, is employed in the present study: if, as a parameter (e.g., $\Delta\mathcal{L}$ or $\mathcal{W}$) increases, a branch enters a bifurcation point, several other branches exit from the point, and precisely one of the exiting branches has the symmetry properties of the original branch, that exiting branch is considered to be the continuation of the entering branch and the others to be higher order branches that originate at the bifurcation point.

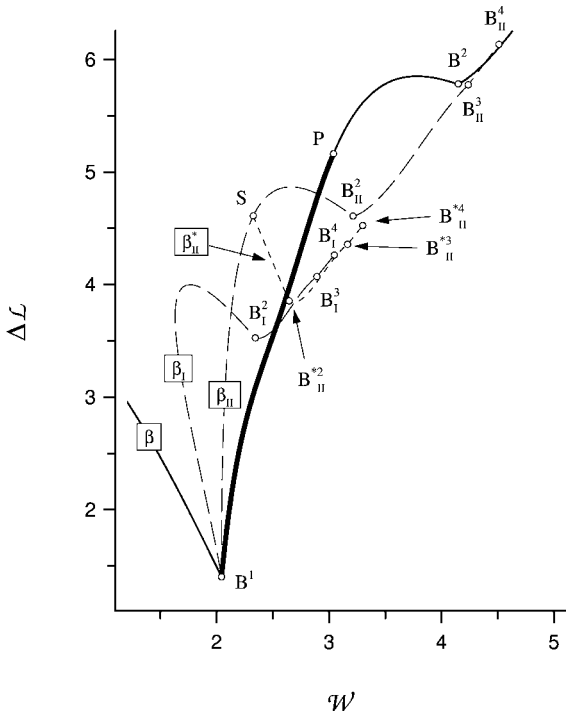

Figure 13. Graphs of $\Delta\mathcal{L}$ versus $\mathcal{W}$ for the secondary branches β_{I}, β_{II} (long dashes) and the tertiary branch β^*_{II} (short dashes).

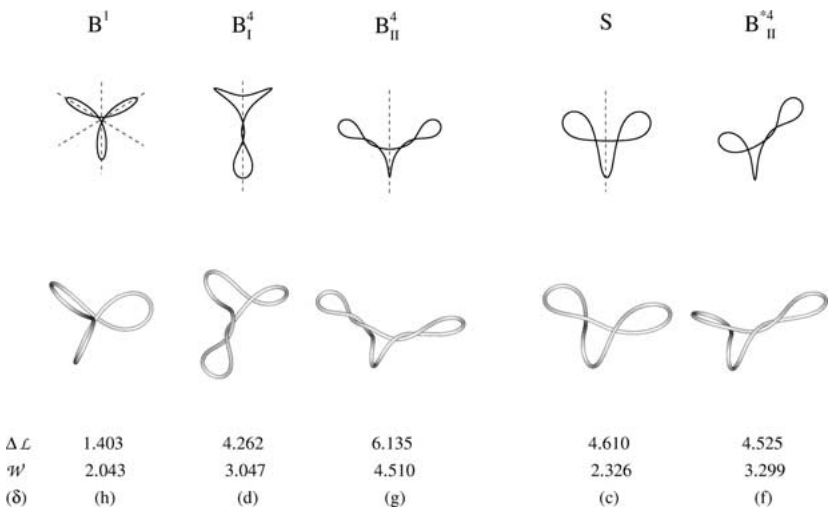

Figure 14. Selected configurations in branches β_{I}, β_{II}, β^*_{II}. S is the configuration at the point of tertiary bifurcation of β_{II}.

As seen in Figure 13, β_{I} and β_{II} originate at B^1, the point in β with the smallest excess link for which self-contact occurs. The configurations in β_{I} have one loop; those in β_{II} have two congruent loops. Our notation is such that, for $n = 1$, 2, or 3, a configuration in β_{I} or β_{II} that has at least one loop with n isolated points of self-contact, but no loop with $n + 1$ such points, lies either in the interval of β_{I} bounded by $\mathrm{B}_{\mathrm{I}}^n$ and $\mathrm{B}_{\mathrm{I}}^{n+1}$ or in the interval of β_{II} bounded by $\mathrm{B}_{\mathrm{II}}^n$ and $\mathrm{B}_{\mathrm{II}}^{n+1}$. The configurations $\mathrm{B}_{\mathrm{I}}^4$ and $\mathrm{B}_{\mathrm{II}}^4$ are shown in Figure 14.

The secondary branch β_{II} has a bifurcation point S at which a tertiary branch, labeled β_{II}^*, originates. The configurations in the tertiary branch have no discernible symmetry; each contains two non-congruent loops (cf. $\mathrm{B}_{\mathrm{II}}^{*4}$ shown in Figure 14). As $\mathcal{W}$ increases, one loop becomes plectonemic, while the other "flattens" (i.e., becomes, in a sense that can be made precise, more planar) and "tightens" (i.e., increases in bending energy).

The point P is the bifurcation point at which β_{III} and β_{IV} originate.* As Figures 14 and 16 make clear, for sufficiently large $\mathcal{W}$ the configurations in β_{III}, like those in β_{I}, have one plectonemic loop and the configurations in β_{IV}, like those in β_{II}, have two such loops. In the range of $\mathcal{W}$ that we consider, the two pairs of branches differ in the following way: Whereas each configuration that is in either β_{III} or β_{IV} has three loops, no configuration in β_{I} or β_{II} has that many loops.

The branch β_{V}, shown in Figure 17, is a closed secondary branch that meets the primary branch β at two bifurcation points: Q and R. Every configuration in β_{V} has three plectonemic loops, each of which shows two points of self-contact. At Q and R, the three loops are congruent, because the configurations are in both β_{V} and β. There are two paths from Q to R in β_{V}. For a configuration on the path containing U, the two congruent loops have less supercoiling than the third; for a configuration on the path containing V, the two congruent loops have more supercoiling than the third (see Figure 18).

With the exception of (closed) branch β_{V} on which $\mathcal{W}$ is bounded, for each primary, secondary, and tertiary branch that we have studied (and also for the isolas discussed below) there is a number $\mathcal{W}^\dagger$ such that for $\mathcal{W} > \mathcal{W}^\dagger$ the configurations in the branch show intervals of self-contact with straight contact curves, while the configurations with $\mathcal{W} \leqslant \mathcal{W}^\dagger$ show at most isolated points of self-contact. The symbol representing the configuration with $\mathcal{W} = \mathcal{W}^\dagger$ has a superscript 4, e.g., A^4, B^4, $\mathrm{B}_{\mathrm{I}}^4$, etc. A configuration with $\mathcal{W}$ near to, but not greater than, $\mathcal{W}^\dagger$ has a loop with 3 points of self-contact. For brevity, the calculations we present for branches other than α are restricted to cases in which $\mathcal{W} \leqslant \mathcal{W}^\dagger$.

* The configuration P is nearly planar and has one point of self-contact in each of its three congruent loops.

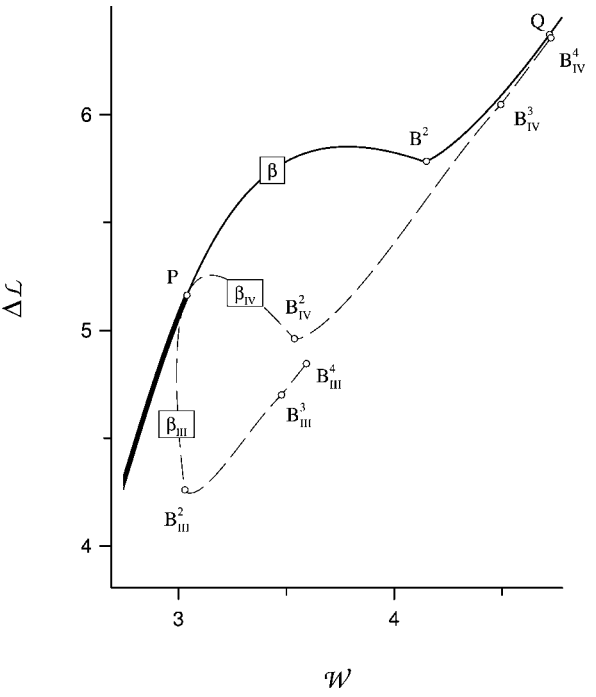

Figure 15. Graphs of $\Delta\mathcal{L}$ versus $\mathcal{W}$ for the secondary branches β_{III} and β_{IV} (dashed curves).

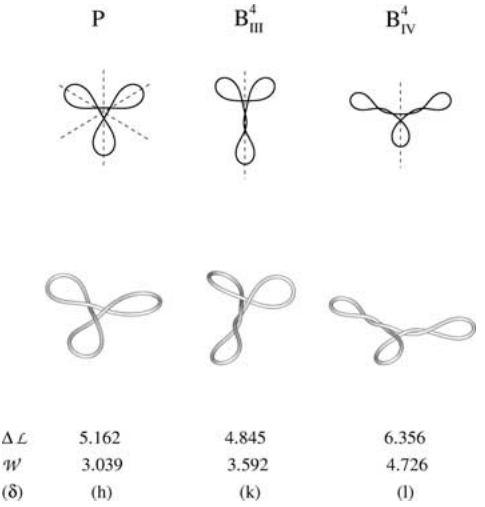

Figure 16. Selected configurations in β_{III} and β_{IV}.

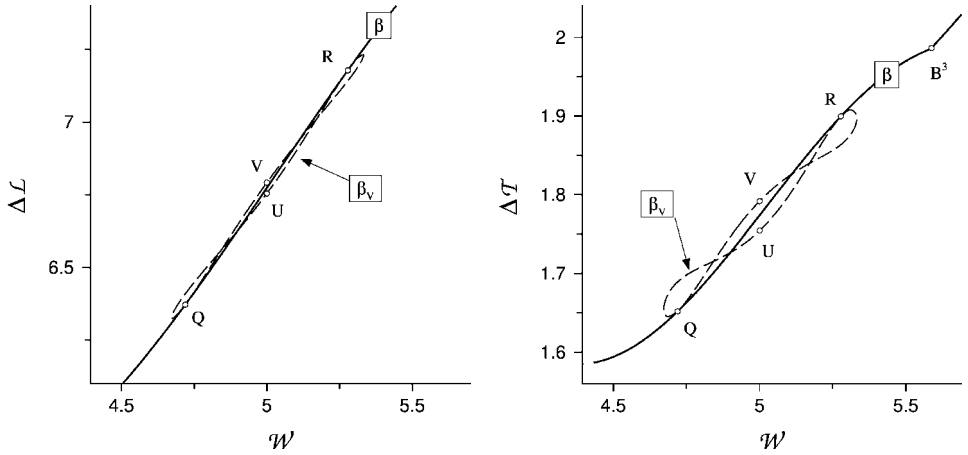

Figure 17. Graphs of $\Delta\mathcal{L}$ versus $\mathcal{W}$ and $\Delta\mathcal{T}$ versus $\mathcal{W}$ for the closed secondary branch β_V (dashed curve). Here, as in Figures 20 and 22, the graph of $\Delta\mathcal{T}$ versus $\mathcal{W}$ is presented to clarify details. U and V are the configurations in β_V with $\mathcal{W} = 5$.

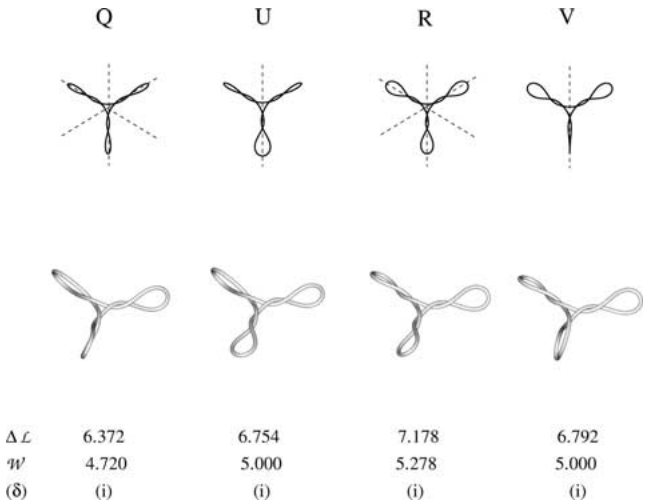

$\Delta\mathcal{L}$	6.372	6.754	7.178	6.792
$\mathcal{W}$	4.720	5.000	5.278	5.000
(δ)	(i)	(i)	(i)	(i)

Figure 18. Selected configurations in β_V. Q and R are configurations at points of secondary bifurcation for β.

ISOLAS RELATED TO THE BRANCH β

In addition to the branches β, β_I, β_{II}, β_{II}^*, β_{III}, β_{IV}, and β_V that are connected to the trivial branch by families of equilibrium configurations, we have found five families of equilibrium configurations (labeled $\bar{\beta}_I$, $\bar{\beta}_{II}$, $\bar{\beta}_{II}^*$, $\bar{\beta}_{III}$, $\bar{\beta}_{IV}$) that are *not* connected to the trivial branch by families of equilibrium configurations, but which share with β, β_I, β_{II}, β_{II}^*, β_{III}, β_{IV}, and β_V the property of being comprised of

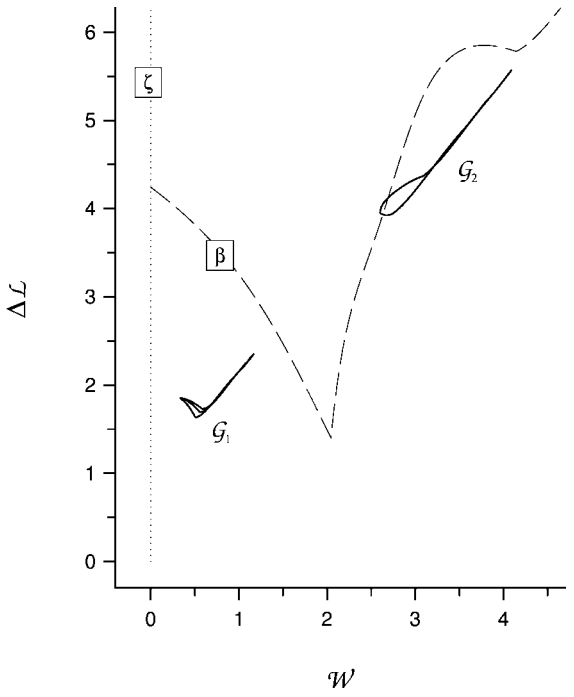

Figure 19. Graphs of $\Delta\mathcal{L}$ versus $\mathcal{W}$ for isolated families of equilibrium configurations (solid curves). Each configuration in these isolated families is unstable. Group $\mathcal{G}_1$ contains the families $\bar{\beta}_{\rm I}$, $\bar{\beta}_{\rm III}$, and $\bar{\beta}^*_{\rm II}$; group $\mathcal{G}_2$ contains $\bar{\beta}_{\rm II}$ and $\bar{\beta}_{\rm IV}$. Here, for clarity, the primary branch β is drawn as a dashed curve.

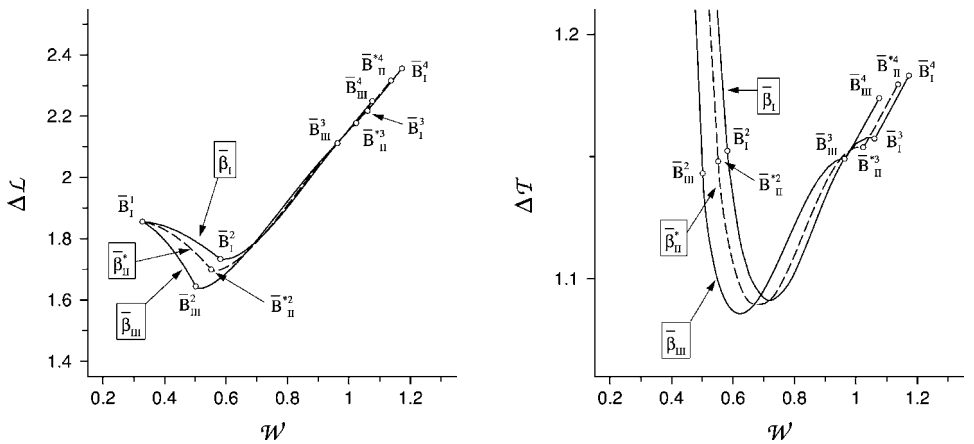

Figure 20. Graphs of $\Delta\mathcal{L}$ versus $\mathcal{W}$ and (with the ordinate much enlarged) $\Delta\mathcal{T}$ versus $\mathcal{W}$ for the isolated families of group $\mathcal{G}_1$, i.e., for $\bar{\beta}_{\rm I}$, $\bar{\beta}_{\rm III}$ (solid curves), and $\bar{\beta}^*_{\rm II}$ (dashed curve). The configuration $\bar{\rm B}^1_{\rm I}$ belongs to each of these families.

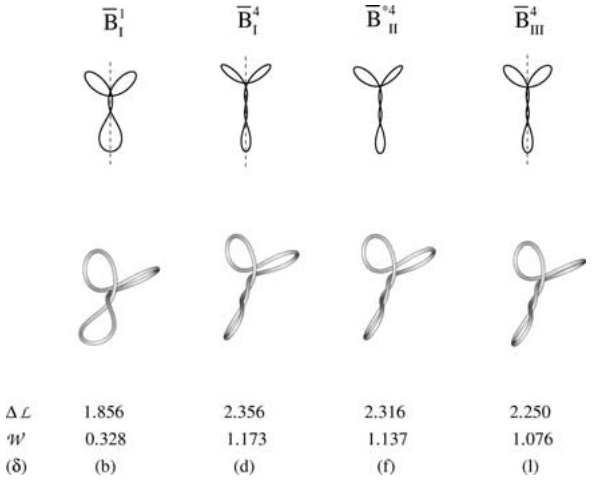

Figure 21. Selected configurations in $\bar{\beta}_{\mathrm{I}}$, $\bar{\beta}_{\mathrm{III}}$, $\bar{\beta}^*_{\mathrm{II}}$.

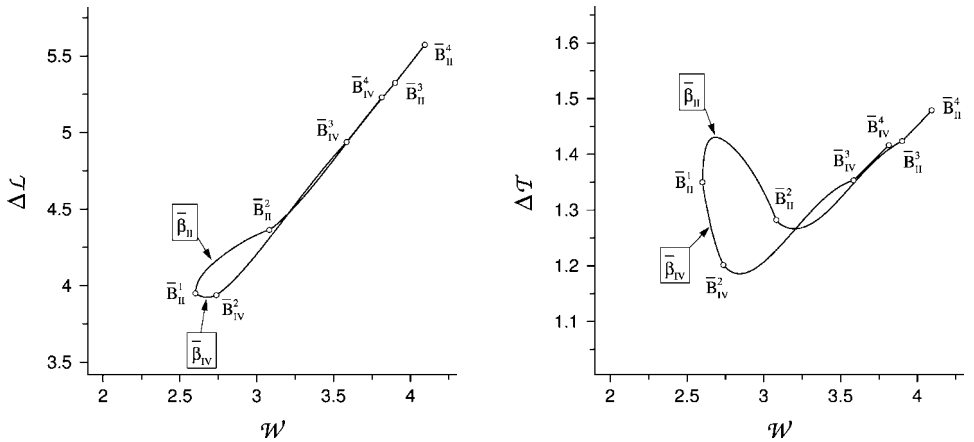

Figure 22. Graphs of $\Delta\mathcal{L}$ versus $\mathcal{W}$ and $\Delta\mathcal{T}$ versus $\mathcal{W}$ for the isolated families of the group $\mathcal{G}_2$, i.e., for $\bar{\beta}_{\mathrm{II}}$ and $\bar{\beta}_{\mathrm{IV}}$. The configuration $\bar{\mathrm{B}}^1_{\mathrm{II}}$ belongs to both families.

configurations for which there are precisely three values of s at which has a local minimum. As seen in Figures 19–23, the *isolated families*, or *isolas*, $\bar{\beta}_{\mathrm{I}}$, $\bar{\beta}_{\mathrm{II}}$, $\bar{\beta}^*_{\mathrm{II}}$, $\bar{\beta}_{\mathrm{III}}$, $\bar{\beta}_{\mathrm{IV}}$ fall naturally into two groups: $\mathcal{G}_1$ containing $\bar{\beta}_{\mathrm{I}}$, $\bar{\beta}^*_{\mathrm{II}}$, $\bar{\beta}_{\mathrm{III}}$ (see Figure 20) and $\mathcal{G}_2$ containing $\bar{\beta}_{\mathrm{II}}$, $\bar{\beta}_{\mathrm{IV}}$ (see Figure 22). The families in $\mathcal{G}_1$ and $\mathcal{G}_2$ share with their corresponding branches β_{I}, β^*_{II}, β_{III}, and β_{II}, β_{IV}, such qualitative properties as symmetry, numbers of loops, and changes in the number of points of self-contact with increasing $\mathcal{W}$. For example, if a configuration is in $\bar{\beta}_{\mathrm{I}}$ or in β_{I}, it has C_2 symmetry and one loop, and if it has $n+1$ points of self-contact, it lies between $\bar{\mathrm{B}}^n_{\mathrm{I}}$ and $\bar{\mathrm{B}}^{n+1}_{\mathrm{I}}$ if it is in $\bar{\beta}_{\mathrm{I}}$ and between $\mathrm{B}^n_{\mathrm{I}}$ and $\mathrm{B}^{n+1}_{\mathrm{I}}$ if it is in β_{I}.

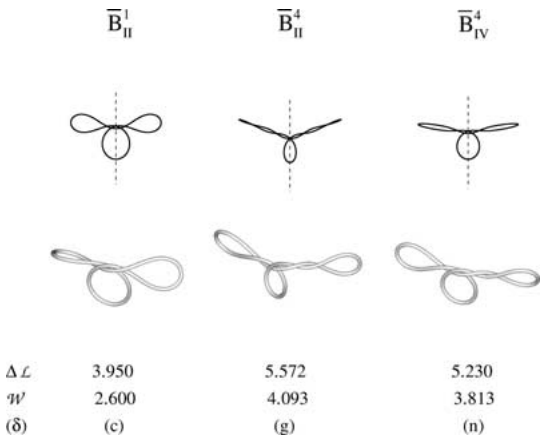

Figure 23. Selected configurations in $\bar{\beta}_{\mathrm{II}}$ and $\bar{\beta}_{\mathrm{IV}}$.

We now have in hand the mathematical apparatus required to discuss the relation between the isolas of Figures 20 and 22 and the secondary bifurcation branches of Figures 13 and 15. We first recall that for each family of equilibrium configurations there is a complementary family in which $\Delta\mathcal{L}$ is replaced by $-\Delta\mathcal{L}$ and $\mathcal{C}$ by its mirror image, and hence $\mathcal{W}$ is replaced by $-\mathcal{W}$ and $\Delta\mathcal{T}$ by $-\Delta\mathcal{T}$. In the discussion that follows we shall show that the mirror image complement of each of the isolas $\bar{\beta}_{\mathrm{I}}$, $\bar{\beta}_{\mathrm{II}}$, $\bar{\beta}^*_{\mathrm{II}}$, $\bar{\beta}_{\mathrm{III}}$, $\bar{\beta}_{\mathrm{IV}}$ is connected by a continuous family of solutions of the equations (1.13)–(1.20) to one of the branches β_{I}, β_{II}, β^*_{II}, β_{III}, β_{IV}.⋆ Each of the connecting families contains a subfamily of solutions that are not configurations because they do not obey condition Γ. For the complements of the isolas $\bar{\beta}_{\mathrm{I}}$, $\bar{\beta}_{\mathrm{II}}$, etc., and the configurations $\overline{\mathrm{B}}^1_{\mathrm{I}}$, $\overline{\mathrm{B}}^4_{\mathrm{I}}$, etc., we shall use the notation ${}^{\mathrm{c}}\bar{\beta}_{\mathrm{I}}$, ${}^{\mathrm{c}}\bar{\beta}_{\mathrm{II}}$, etc., and ${}^{\mathrm{c}}\overline{\mathrm{B}}^1_{\mathrm{I}}$, ${}^{\mathrm{c}}\overline{\mathrm{B}}^4_{\mathrm{I}}$, etc.

When one considers solutions of the system (1.13)–(1.20) but does not confine attention to those that obey conditions Γ and C, each of the points $\mathrm{B}^1_{\mathrm{I}}$, $\mathrm{B}^2_{\mathrm{I}}$, $\mathrm{B}^3_{\mathrm{I}}$, $\mathrm{B}^4_{\mathrm{I}}$ of the branch β_{I} (see Figures 13 and 14), i.e., each of the configurations in that secondary branch at which there is a change in the contact diagram, becomes a bifurcation point at which a new family of solutions originates; the members of the new family, $\tilde{\beta}^n_{\mathrm{I}}$, $n = 1, 2, 3$, have the C_2 symmetry of configurations in β_{I}. The extended bifurcation diagram obtained in this way is presented in Figure 24 as a graph of Ψ versus $\Delta\mathcal{T}$. For each member of the families $\tilde{\beta}^1_{\mathrm{I}}$ and $\tilde{\beta}^2_{\mathrm{I}}$ there is one point at which the relation (1.15) holds; there are two such points for each member of $\tilde{\beta}^3_{\mathrm{I}}$, and three for each member of $\tilde{\beta}^4_{\mathrm{I}}$. For each n, the family $\tilde{\beta}^n_{\mathrm{I}}$ connects the configurations $\mathrm{B}^n_{\mathrm{I}}$ and ${}^{\mathrm{c}}\overline{\mathrm{B}}^n_{\mathrm{I}}$, and hence connects the isola ${}^{\mathrm{c}}\bar{\beta}_{\mathrm{I}}$ to the secondary branch β_{I}.

⋆ In a theory of planar configurations of rods constrained by impenetrable walls, a phenomenon of this type (in which isolas are connected to the trivial branch by families of configurations that violate the condition of impenetrability) was found and analyzed by Holmes et al. [21].

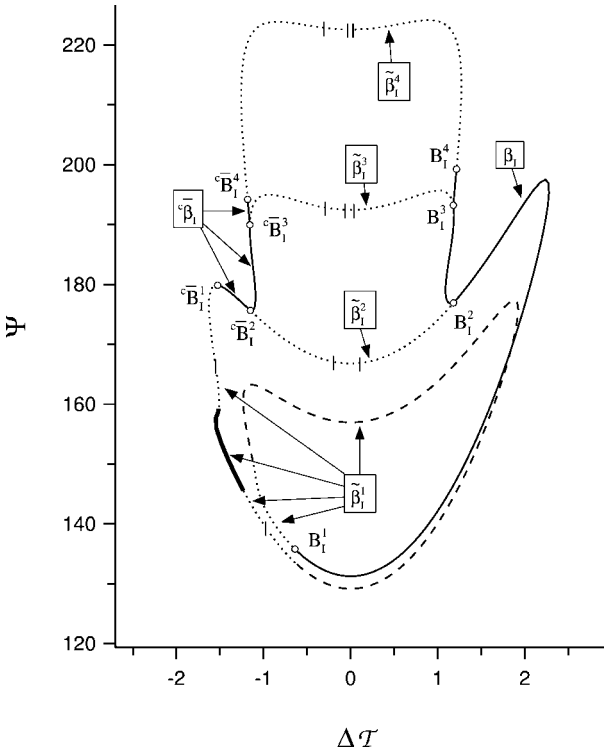

Figure 24. Graphs of Ψ versus $\Delta\mathcal{T}$ for the families β_{I} and ${}^{\mathrm{c}}\bar{\beta}_{\mathrm{I}}$, and for the families $\tilde{\beta}_{\mathrm{I}}^{1}$, $\tilde{\beta}_{\mathrm{I}}^{2}$, $\tilde{\beta}_{\mathrm{I}}^{3}$, $\tilde{\beta}_{\mathrm{I}}^{4}$ (containing unphysical solutions of (1.13)–(1.20)) that connect ${}^{\mathrm{c}}\bar{\beta}_{\mathrm{I}}$ to β_{I}. The following notation is used here and in Figures 25–28 below: Subfamilies that contain only solutions that fail to obey condition Γ (and hence are such that $\mathcal{R}$ penetrates itself) are shown as dotted curves. Subfamilies that contain only solutions that do obey condition Γ but fail to obey condition C (and hence are not equilibrium configurations) are shown as dashed lines. The subfamily of $\tilde{\beta}_{\mathrm{I}}^{1}$ whose members obey both Γ and C but have axial curves that are trefoil knots is shown as a heavy solid line. Vertical bars label configurations in which $\mathcal{C}$ intersects itself.

The retention of solutions of (1.13)–(1.20) that do not obey Γ or C enables us to construct also the following families: $\tilde{\beta}_{\mathrm{II}}^{*n}$, $n = 2, 3, 4$, connecting the isola ${}^{\mathrm{c}}\bar{\beta}_{\mathrm{II}}^{*}$ to the tertiary branch β_{II}^{*} (see Figure 25); $\tilde{\beta}_{\mathrm{II}}^{n}$, $n = 2, 3, 4$, connecting the isola ${}^{\mathrm{c}}\bar{\beta}_{\mathrm{II}}$ to the secondary branch β_{II} (see Figure 26); $\tilde{\beta}_{\mathrm{III}}^{n}$, $n = 2, 3, 4$, connecting the isola ${}^{\mathrm{c}}\bar{\beta}_{\mathrm{III}}$ to the secondary branch β_{III} (see Figure 27); and $\tilde{\beta}_{\mathrm{IV}}^{n}$, $n = 2, 3, 4$, connecting the isola ${}^{\mathrm{c}}\bar{\beta}_{\mathrm{IV}}$ to the secondary branch β_{IV} (see Figure 28).

The family of solutions $\hat{\beta}_{\mathrm{II}}^{*1}$ connects the configuration ${}^{\mathrm{c}}\overline{\mathrm{B}}_{\mathrm{II}}^{*1}$ to its mirror image $\overline{\mathrm{B}}_{\mathrm{II}}^{*1}$ (which is identical to the configuration $\overline{\mathrm{B}}_{\mathrm{I}}^{1}$ shown in Figure 21), i.e., connects the complementary isolas $\bar{\beta}_{\mathrm{II}}^{*}$ and ${}^{\mathrm{c}}\bar{\beta}_{\mathrm{II}}^{*}$. One-half of that family is shown in Figure 25; the region of $\hat{\beta}_{\mathrm{II}}^{*1}$ seen there originates at ${}^{\mathrm{c}}\overline{\mathrm{B}}_{\mathrm{II}}^{*1}$ and terminates at a point labeled Δ that corresponds to a solution with $\Delta\mathcal{T} = 0$ and $\mathcal{C}$ a planar curve that crosses itself; the region of $\hat{\beta}_{\mathrm{II}}^{*1}$ connecting Δ to $\overline{\mathrm{B}}_{\mathrm{II}}^{*1}$ is complementary to the region

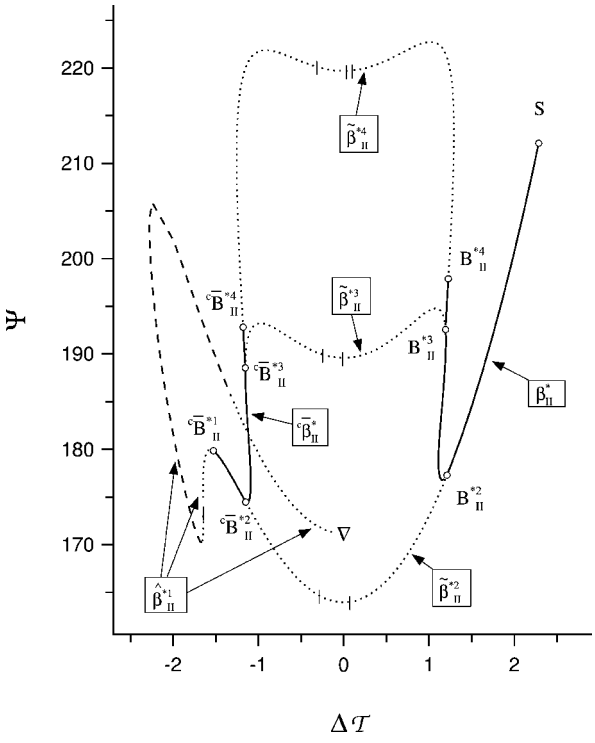

Figure 25. Graphs of Ψ versus $\Delta\mathcal{T}$ for the families $\beta^*_{\rm II}$ and ${}^{\rm c}\bar{\beta}^*_{\rm II}$, and the families $\tilde{\beta}^{*2}_{\rm II}$, $\tilde{\beta}^{*3}_{\rm II}$, $\tilde{\beta}^{*4}_{\rm II}$ that connect ${}^{\rm c}\bar{\beta}^*_{\rm II}$ to $\beta^*_{\rm II}$. Also shown is a region of the family $\hat{\beta}^{*1}_{\rm II}$ that connects ${}^{\rm c}\bar{\beta}^*_{\rm II}$ to its mirror-image complement $\bar{\beta}^*_{\rm II}$. Here, and also Figure 26, the point marked Δ corresponds to a solution with $\Delta\mathcal{T} = 0$ and $\mathcal{C}$ a planar curve.

shown, i.e., each solution lying in one is a (mirror image) complement of a solution lying in the other. A similar situation occurs in Figure 26 where a region is shown of the family $\hat{\beta}^1_{\rm II}$ that connects ${}^{\rm c}\overline{\rm B}^1_{\rm II}$ to its complement $\overline{\rm B}^1_{\rm II}$ (shown in Figure 23), i.e., connects the isola ${}^{\rm c}\bar{\beta}_{\rm II}$ to its complement $\bar{\beta}_{\rm II}$.

The family $\breve{\beta}^1_{\rm II}$ of Figure 26 originates at $\rm B^1_{II}$ and appears in the figure as an open curve that terminates at the point labeled $\otimes$, for which the corresponding solution of (1.13)–(1.20) is such that $\mathcal{C}$ has a helical subsegment. A similar situation holds for the family $\breve{\beta}^1_{\rm III}$ of Figure 27, which originates at $\rm B^1_{III}$, and the family $\breve{\beta}^1_{\rm IV}$ of Figure 28, which originates at $\rm B^1_{IV}$. The symbol $\otimes$ refers to different solutions in each of these figures; the property that they have in common is the presence of a helical subsegment for which the sextuple $(a_i, \lambda_i, T_i, \sigma_i^-, \sigma_i^+, L_i)$ lies at the boundary of the region in parameter space for which the roots $u_{1,i}, u_{2,i}, u_{3,i}$ of the cubic P_i in (2.13) are real. It is not at present clear how the graphs shown may be extended beyond a point corresponding to such a solution.

REMARK. Of the several one-parameter families of solutions of (1.13)–(1.20) that we have found to connect an isola to a branch (i.e., to family of configurations

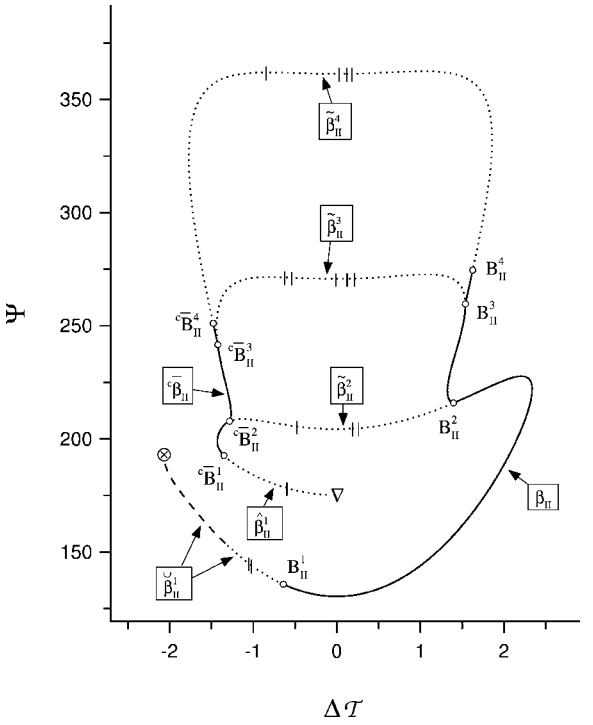

Figure 26. Graphs of Ψ versus $\Delta\mathcal{T}$ for the families $\beta_{\rm II}$ and ${}^{\rm c}\bar{\beta}_{\rm II}$, and the families $\tilde{\beta}^2_{\rm II}$, $\tilde{\beta}^3_{\rm II}$, $\tilde{\beta}^4_{\rm II}$ that connect ${}^{\rm c}\bar{\beta}_{\rm II}$ to $\beta_{\rm II}$. Also shown is the family $\hat{\beta}^1_{\rm II}$ that connects ${}^{\rm c}\bar{\beta}_{\rm II}$ to $\bar{\beta}_{\rm II}$, and a family $\check{\beta}^1_{\rm II}$ that originates at $\mathrm{B}^1_{\rm II}$ and has been calculated up to a point labeled $\otimes$. Here, and also in Figures 27 and 28, the label $\otimes$ indicates that the point corresponds to a solution of (1.13)–(1.20) for which $\mathcal{C}$ has a helical subsegment.

arising by successive bifurcations from the trivial branch) or to another isola, all contain solutions at which $\mathcal{C}$ passes through itself, and only two, $\tilde{\beta}^1_{\rm I}$ (which connects ${}^{\rm c}\bar{\beta}_{\rm I}$ to $\beta_{\rm I}$) and $\hat{\beta}^{*1}_{\rm II}$ (which connects ${}^{\rm c}\bar{\beta}^*_{\rm II}$ to $\bar{\beta}^*_{\rm II}$), have subfamilies in which condition Γ holds. Both $\tilde{\beta}^1_{\rm I}$ and $\hat{\beta}^{*1}_{\rm II}$ begin and end with subfamilies that fail to obey Γ and hence are shown as dotted curves in Figures 24 (for $\tilde{\beta}^1_{\rm I}$) and 25 (for $\hat{\beta}^{*1}_{\rm II}$). The family $\tilde{\beta}^1_{\rm I}$ has two subfamilies in which Γ holds; in one of these subfamilies condition C does not hold, in the other both Γ and C hold but the axial curve $\mathcal{C}$ is a trefoil knot. The family $\hat{\beta}^{*1}_{\rm II}$ has two subfamilies in which condition Γ holds but C does not.

PRIMARY BRANCH γ

The primary branch γ (see Figures 1 and 29), which originates at the point C^0 on ζ where $\Delta\mathcal{L} = \sqrt{15}/\omega$, has index 3 and hence is comprised of configurations with D_4 symmetry. The configurations in γ between C^0 and C^1 are free from self-contact; those between C^1 and C^2 have 4 congruent loops, each of which makes

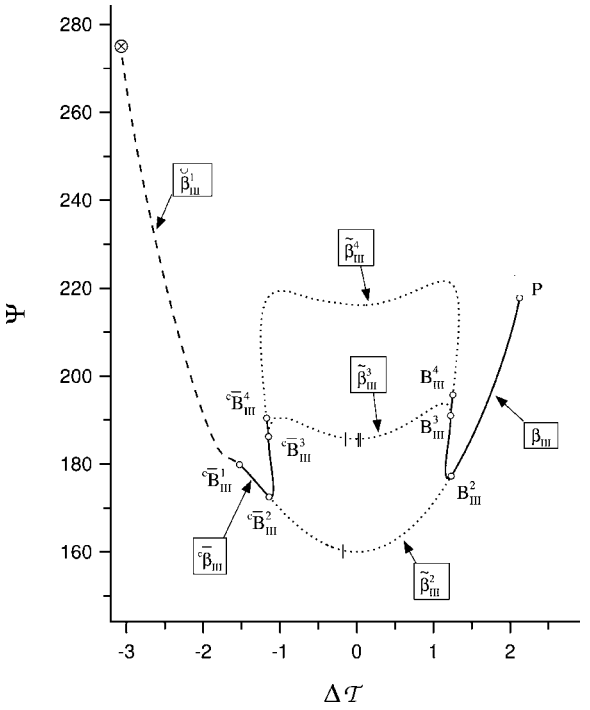

Figure 27. Graphs of Ψ versus $\Delta\mathcal{T}$ for the families $\beta_{\rm III}$ and ${}^{\rm c}\bar{\beta}_{\rm III}$, and the families $\tilde{\beta}^2_{\rm III}$, $\tilde{\beta}^3_{\rm III}$, $\tilde{\beta}^4_{\rm III}$ that connect ${}^{\rm c}\bar{\beta}_{\rm III}$ to $\beta_{\rm III}$. Also shown is a family $\breve{\beta}^1_{\rm III}$ that connects ${}^{\rm c}\bar{\rm B}^1_{\rm III}$ to a point with the label $\otimes$.

one contact with itself. The bifurcation occurring at $\rm C^1$ gives rise to four secondary branches, labeled $\gamma_{\rm I}$, $\gamma_{\rm II}$, $\gamma_{\rm III}$, $\gamma_{\rm IV}$. Whereas the configurations in $\gamma_{\rm I}$, $\gamma_{\rm II}$, and $\gamma_{\rm IV}$ have C_2 symmetry, those in $\gamma_{\rm III}$ have D_2 symmetry. We have not extended our calculations for these branches beyond the range of $\mathcal{W}$ for which curves are shown in Figure 30, i.e., the range in which each loop has less than two points of self-contact.

It is interesting to note that although the configurations in $\gamma_{\rm II}$ and $\gamma_{\rm III}$ have different symmetry groups, they give rise to the same graph of $\Delta\mathcal{L}$ versus $\mathcal{W}$, which is a consequence of the fact that to each configuration in $\gamma_{\rm II}$ there corresponds a configuration in $\gamma_{\rm III}$ that can be obtained from the former by first cutting $\mathcal{R}$ at each of its four cross-sections that are at points of minimum curvature κ and then rearranging the resulting pair-wise congruent segments into a configuration with D_2, rather than C_2, symmetry. (Consider, for example, the configurations $\rm C^2_{II}$ (with C_2 symmetry) and $\rm C^2_{III}$ (with D_2 symmetry) that have equal values of $\Delta\mathcal{L}$ and $\mathcal{W}$ and are shown in Figure 30.)

ON THE STABILITY OF THE CALCULATED CONFIGURATIONS

The stability of circular configurations, i.e., those in the trivial branch ζ, is discussed in detail in Appendix B to [2], where a rigorous proof is given of the

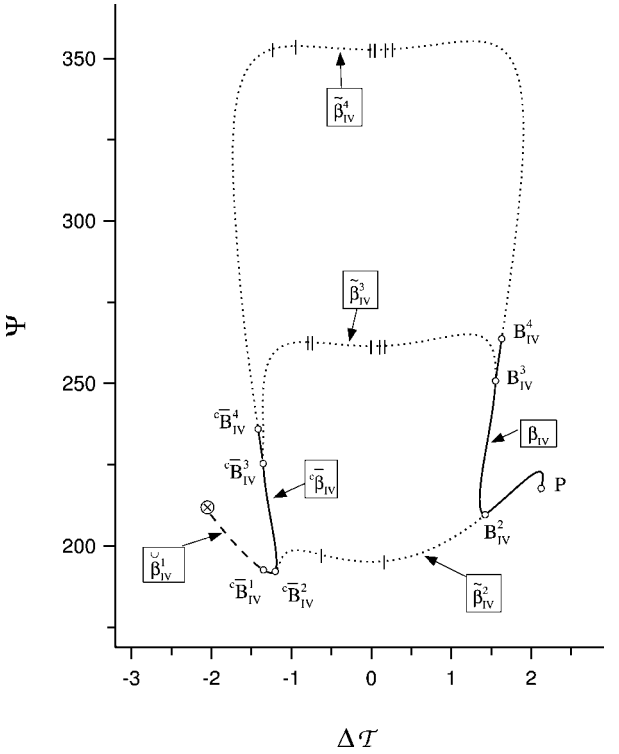

Figure 28. Graphs of Ψ versus $\Delta\mathcal{T}$ for the families β_{IV} and ${}^c\bar{\beta}_{IV}$, and the families $\tilde{\beta}^2_{IV}$, $\tilde{\beta}^3_{IV}$, $\tilde{\beta}^4_{IV}$ that connect ${}^c\bar{\beta}_{IV}$ to β_{IV}. Also shown is a family $\breve{\beta}^1_{IV}$ that connects ${}^cB^1_{IV}$ to a point with the label $\otimes$.

assertion that the unstable configurations in ζ are those for which $\Delta\mathcal{L}$ is above its value at A^0; i.e., that each circular configuration with $\Delta\mathcal{L} < \sqrt{3}/\omega$ is stable and each with $\Delta\mathcal{L} > \sqrt{3}/\omega$ is unstable.*

The branch α originates at A^0. On α, $d\Delta\mathcal{L}/d\mathcal{W}$ at $\mathcal{W} = 0$ is a strictly monotone increasing function of ω and vanishes when $\omega = 11/8$;** hence the configuration A^0 is stable if $\omega > 11/8$ and unstable if $\omega \leqslant 11/8$.‡ As we pointed out earlier in this section, use of the conditions E and S permits one to give a full analysis of the stability of configurations in α, and to show that such a configuration is stable if, for it, $d\Delta\mathcal{L}/d\mathcal{W} > 0$.

* Of course, we here take $\Delta\mathcal{L}$ and $\mathcal{W}$ to be non-negative.

** The result that $d\Delta\mathcal{L}/d\mathcal{W} = 0$ at $\mathcal{W} = 0$ when $\omega = 11/8$ follows from equation (15) of [2].

‡ These results are independent of the value of d and imply that (i) there is a critical value of $\omega^{\#}$ ω such that for $\omega > \omega^{\#}$ there is in α region of contact-free configurations that are stable and for $\omega \leqslant \omega^{\#}$ there is no such region and (ii) $\omega^{\#}$ equals 11/8, in contradiction to an assertion on page 7243 of [33] to the effect that $\omega^{\#} = 1$. Matters related to the dependence of the stability of configurations on ω are discussed in detail in [2].

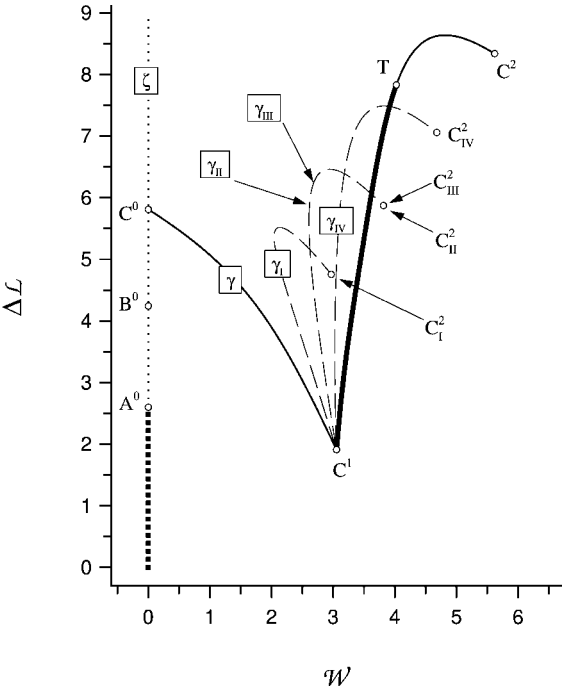

Figure 29. Graphs of $\Delta\mathcal{L}$ versus $\mathcal{W}$ for the primary branch γ and the secondary branches γ_{I}, γ_{II}, γ_{III}, and γ_{IV}. The graphs for γ_{II} and γ_{III} are identical. C^1 and T are bifurcation points for γ.

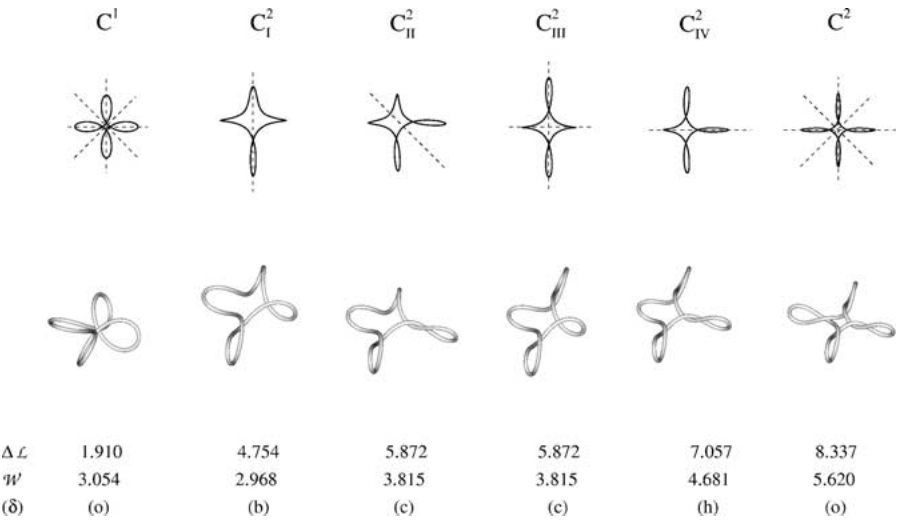

Figure 30. Selected configurations in branches γ, γ_{I}, γ_{II}, γ_{III}, and γ_{IV}. As explained in the text, C^2_Ξ, with $\Xi = \mathrm{I}, \mathrm{II}, \mathrm{III}, \mathrm{IV}$, is the configuration of largest writhe in the branch γ_Ξ with at most 1 point of self-contact in each loop.

For each of the secondary branches, tertiary branches, and isolas studied in this paper,* the corresponding configurations fail to obey condition θ and hence are unstable.** In other words, our calculations indicate that, for the range of parameters we have studied, for a configuration to be stable it is necessary that it be either on the trivial branch or on a primary bifurcation branch.

The regions of primary branches comprised of unstable configurations are shown as lightface solid curves in Figures 3–6, 11, 13, 15, 17, and 29. As condition W is difficult to verify on branches other than α, it is not feasible to use condition S to locate the stable configurations in branches β and γ. The regions of the branches β and γ in which configurations obey the strict form of condition θ are shown as heavy solid lines in Figures 3–5, 11, 13, 15 and 29. Each such configuration obeys the relation (3.11) in addition to the inequality $\theta(\zeta) > 0$ (for $0 < \zeta \leqslant L$). As it can be shown that each configuration without points of self-contact that obeys the strict form of condition θ is differentially stable, we conjecture that, even for configurations in which self-contact occurs, the strict form of condition θ is a sufficient for, at the least, differential stability.

DEPENDENCE OF CONFIGURATIONS ON THE RATIO C/A

Reference [1] contains a derivation of an expression for the dependence of bifurcation diagrams on C and A, which, under our assumption that long range forces are not present, reduces to the following assertion: For each fixed value of $d = D/L$, the graphs of $\Delta\mathcal{L}$ versus $\mathcal{W}$ for two distinct values, ω_1, ω_2, of $\omega = C/A$ are such that vertical distances from the line $\Delta\mathcal{L} = \mathcal{W}$ are inversely proportional to ω:

$$[\Delta\mathcal{L}(\mathcal{W}, \omega_2) - \mathcal{W}]\omega_2 = [\Delta\mathcal{L}(\mathcal{W}, \omega_1) - \mathcal{W}]\omega_1. \tag{4.3}$$

Indeed, there is a correspondence between equilibrium configurations of closed rods of specified D and L that differ in their values of ω and $\Delta\mathcal{L}$. The corresponding configurations have the same value of $\mathcal{W}$ (and, in fact, the same $\mathcal{C}$) and, in accord with (4.3), also the same value of $\omega\Delta\mathcal{T}$.

To obtain Figure 31, which shows primary bifurcation branches for the case $\omega = 8/5$, we have employed equation (4.3) and Figure 3, which shows the same branches when $\omega = 2/3$. As in Figure 3, the regions of primary branches in which configurations are unstable are drawn as light curves, and the regions in which configurations obey the strict form of condition θ are drawn as heavy curves.

Although the graphs of Ψ_B versus $\mathcal{W}$ shown in Figure 4 are invariant under changes in ω, the stability of configurations in regions of those graphs is not, but is to be investigated by the methods discussed above. Results for the case $\omega = 8/5$ are shown in Figure 32. As 8/5 exceeds 11/8, the critical value of ω for the occurrence

* E.g., β_{I}, β_{II}, β_{III}, β_{IV}, β_{V}, β^*_{II}, $\bar{\beta}_{\mathrm{I}}$, $\bar{\beta}_{\mathrm{II}}$, $\bar{\beta}_{\mathrm{III}}$, $\bar{\beta}_{\mathrm{IV}}$, $\bar{\beta}^*_{\mathrm{II}}$, γ_{I}, γ_{II}, γ_{III}, γ_{IV}. These higher-order branches and isolas are shown in Figures 13, 15, 17, 20, 22, 29.

** For examples of graphs of θ versus ζ for configurations that obey or fail to obey condition θ see Figure 7 of [2].

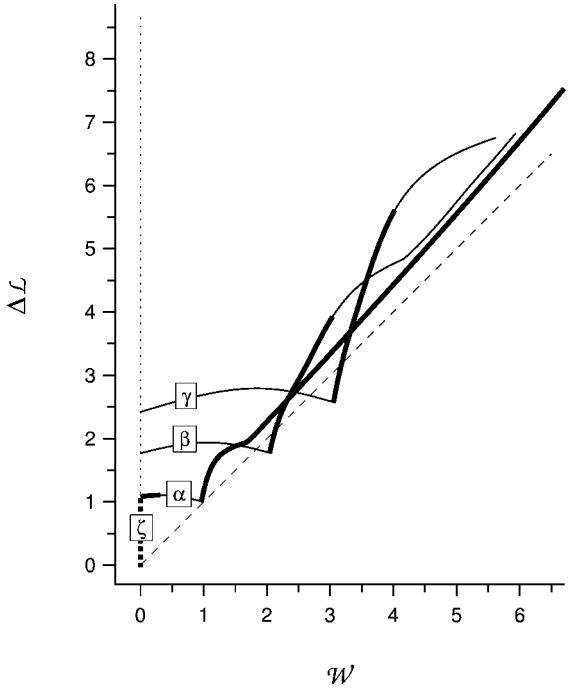

Figure 31. Bifurcation diagram for a closed rod with $\omega = 8/5$, drawn as a plot of $\Delta\mathcal{L}$ versus $\mathcal{W}$, and showing branches $\zeta, \alpha, \beta, \gamma$.

in α of a contact-free point of exchange of stability, in each of the Figures 31, 32, and 33 there is a short region of that branch (starting at ζ, i.e., at A^0) that is comprised of configurations that are not only contact-free and non-circular, but also stable.⋆ In the present case, as in the case $\omega = 2/3$, each configuration that we have studied that lies in a secondary or tertiary branch or in an isola does not obey condition θ and hence is unstable.

As was pointed out in [2],⋆⋆ Figures 3 and 31 can be obtained from Figure 4 (or Figure 32) by use of the relation (3.8). Of course, once Ψ_B is known as a function of $\mathcal{W}$ and $\Delta\mathcal{L}$ is known as a function of $\mathcal{W}$, one can easily construct graphs of Ψ versus $\Delta\mathcal{L}$, such as those shown in Figures 5 and 33.

Acknowledgements

This research was supported by the National Science Foundation under Grant DMS-97-05016. David Swigon acknowledges with gratitude a Fellowship from the Program in Mathematics and Molecular Biology with funding from the Burroughs Wellcome Fund Interfaces Program.

⋆ Cf. footnote ⋆ on page 215.

⋆⋆ See the paragraph containing equation (13) of that paper.

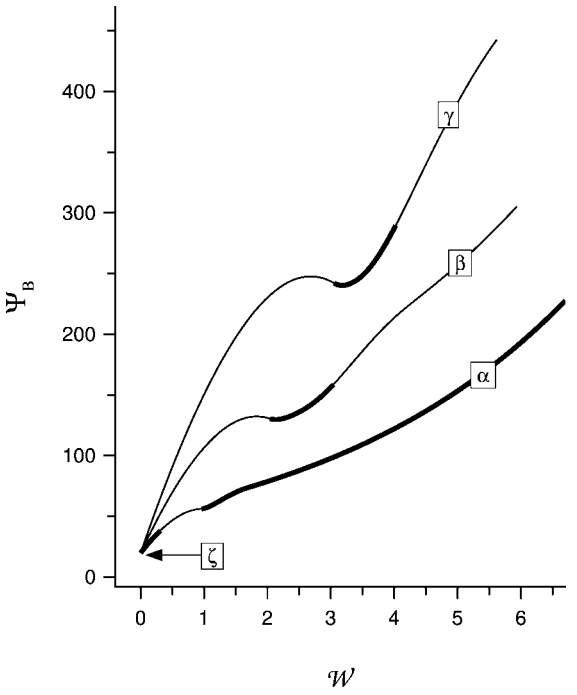

Figure 32. Graphs of Ψ_B versus $\mathcal{W}$ for the primary branches α, β, γ when $\omega = 8/5$. A comparison with Figure 4 illustrates the fact that, for fixed d and L, although graphs of Ψ_B versus $\mathcal{W}$ are independent of ω, the range of values of $\mathcal{W}$ for which configurations in a primary branch are stable increases with increasing ω.

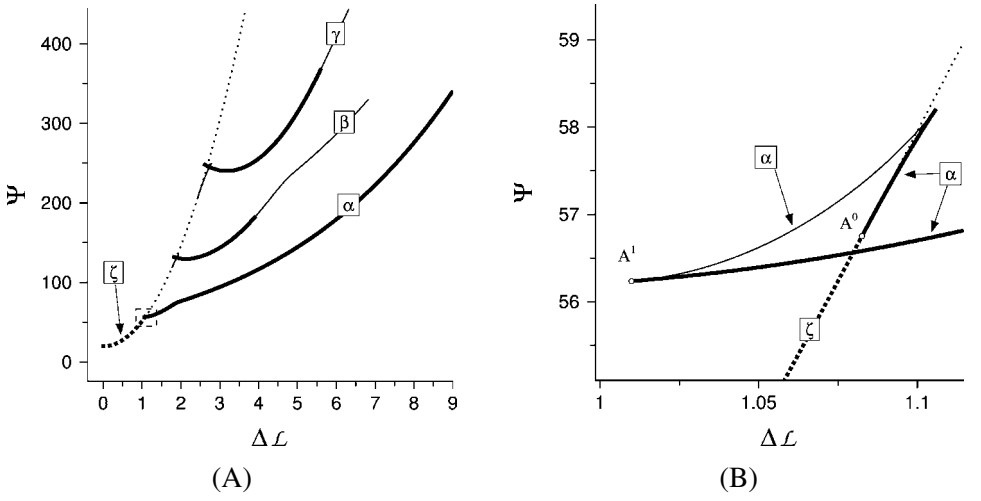

Figure 33. (A) Graphs of Ψ versus $\Delta\mathcal{L}$ for branches ζ, α, β, γ when $\omega = 8/5$. (B) An enlargement of the rectangular region containing A^0 and A^1. This figure should be compared with Figure 5 where $\omega = 2/3$.

References

1. I. Tobias, D. Swigon, and B.D. Coleman, Elastic stability of DNA configurations: I. General theory. *Phys. Rev. E* **61** (2000) 747–758.
2. B.D. Coleman, D. Swigon, and I. Tobias, Elastic stability of DNA configurations: II. Supercoiling of miniplasmids. *Phys. Rev. E* **61** (2000) 759–770.
3. D. Swigon, Configurations with self-contact in the theory of the elastic rod model for DNA, Doctoral Dissertation, Rutgers University, New Brunswick (1999).
4. G. Kirchhoff, Über das Gleichgewicht und die Bewegung eines unendlich dünen elastischen Stabes. *J. Reine angew. Math. (Crelle)* **56** (1859) 285–313.
5. A. Clebsch, *Theorie der Elasticität Fester Körper*, Teubner, Leipzig (1862).
6. G. Kirchhoff, *Vorlesungen über mathematische Physik, Mechanik*, Vol. 28, Teubner, Leipzig (1876).
7. E.H. Dill, Kirchhoff's theory of rods. *Arch. Hist. Exact Sci.* **44** (1992) 1–23.
8. R. Courant, *Differential and Integral Calculus*, Vol. II, Blackie, London (1936).
9. F.B. Fuller, The writhing number of a space curve. *Proc. Natl. Acad. Sci. USA.* **68** (1971) 815–819.
10. J.H. White, An introduction to the geometry and topology of DNA structure. In: *Mathematical Methods for DNA Sequences*, CRC, Boca Raton, Florida (1989), pp. 225–253.
11. G. Calugareanu, Sur les classes d'isotopie des noeuds tridimensionnels et leurs invariants. *Czechoslovak Math. J.* **11** (1961) 588–625.
12. J.H. White, Self-linking and the Gauss integral in higher dimensions. *Amer. J. Math.* **91** (1969) 693–728.
13. R.A. Litherland, J. Simon, O. Durumeric, and E. Rawdon, Thickness of knots. *Topology Appl.* **91** (1999) 233–244.
14. M. Le Bret, Twist and writhing in short circular DNAs according to first-order elasticity. *Biopolymers* **23** (1984) 1835–1867.
15. L.D. Landau and E.M. Lifshitz, *Theory of Elasticity*, Pergamon Press, Oxford (1959).
16. I. Tobias, B.D. Coleman, and W. Olson, The dependence of DNA tertiary structure on end conditions: Theory and implications for topological transitions. *J. Chem. Phys.* **101** (1994) 10990–10996.
17. B.D. Coleman, I. Tobias, and D. Swigon, Theory of the influence of end conditions on self-contact in DNA loops. *J. Chem. Phys.* **103** (1995) 9101–9109.
18. D. Swigon, B.D. Coleman, and I. Tobias, The elastic rod model for DNA and its application to the tertiary structure of DNA minicircles in mononucleosomes. *Biophys. J.* **74** (1998) 2515–2530.
19. B.D. Coleman, E.H. Dill, M. Lembo, Z. Lu, and I. Tobias, On the dynamics of rods in the theory of Kirchhoff and Clebsch. *Arch. Rational Mech. Anal.* **121** (1993) 339–359.
20. J.W. Milnor, *Topology from the Differentiable Viewpoint*, 2nd edn, The University Press of Virginia, Charlotesville (1969).
21. P.J. Holmes, G. Domokos, J. Schmitt, and I. Szeberényi, Constrained Euler buckling: An interplay of computation an analysis. *Comp. Meth. in Appl. Mech. and Eng.* **170** (1999) 175–207.
22. W.F. Pohl, The self-linking number of a closed space curve. *J. Math. Mech.* **17** (1968) 975–985.
23. P.J. Hagerman, Flexibility of DNA. *Annu. Rev. Biophys. Biophys. Chem.* **17** (1988) 265–286.
24. J.M. Schurr, B.S. Fujimoto, P. Wu, and L. Song, Fluorescence studies of nucleic acids: Dynamics, rigidities, and structures. In: J.R. Lakowicz (ed.), *Topics in Fluorescence Spectroscopy, Vol. 3: Biochemical Applications*, Plenum Press, New York (1992).
25. D.S. Horowitz and J.C. Wang, Torsional rigidity of DNA and length dependence of the free energy of DNA supercoiling. *J. Mol. Biol.* **173** (1984) 75–91.
26. C. Bouchiat and M. Mezard, Elasticity model of supercoiled DNA molecule. *Phys. Rev. Lett.* **80** (1998) 1556–1559.

27. T. R. Strick, J.-F. Allemand, D. Bensimon, A. Bensimon, and V. Croquette, The elasticity of a single supercoiled DNA molecule. *Science* **271** (1996) 1835–1837.
28. P.J. Heath, J.B. Clendenning, B.S. Fujimoto, and J.M. Schurr, Effect of bending strain on the torsion elastic constant of DNA. *J. Mol. Biol.* **260** (1996) 718–730.
29. E.E. Zajac, Stability of two planar loop elasticas. *J. Appl. Mech.* **29** (1962) 136–142.
30. G. Domokos, A group-theoretic approach to the geometry of elastic rings. *J. Nonlinear Sci.* **5** (1995) 453–478.
31. G. Domokos and T.J. Healey, Hidden symmetry of global solutions in twisted elastic rings. *J. Nonlin. Sci.* (October 2000), accepted.
32. D.M. Stump, W.B. Fraser, and K.E. Gates, The writhing of circular cross-section rods: From undersea cables to DNA supercoils. *Proc. Roy. Soc. London* **A 454** (1998) 2123–2156.
33. B. Fain and J. Rudnick, Conformations of closed DNA. *Phys. Rev. E* **60** (1999) 7239–7252.